Trabecular and cortical bone structure of the talus and distal tibia in *Pan* and *Homo*

Zewdi J. Tsegai [1*], Matthew M. Skinner [2, 1], Andrew H. Gee [3], Dieter H. Pahr [4], Graham M. Treece [3], Jean-Jacques Hublin [1], Tracy L. Kivell [2, 1]

Affiliations

[1] Department of Human Evolution, Max Planck Institute for Evolutionary Anthropology

[2] Skeletal Biology Research Centre, School of Anthropology and Conservation, University of Kent

[3] Department of Engineering, University of Cambridge

[4] Institute for Lightweight Design and Structural Biomechanics, Vienna University of Technology

* Corresponding author:

Zewdi Tsegai

Max Planck Institute for Evolutionary Anthropology

Department of Human Evolution

Deutscher Platz 6

D-04103 Leipzig

Germany

Abbreviated title: Internal bone structure of talus and tibia

Keywords: Bone microstructure, Functional morphology, Locomotion, Bipedalism, Cancellous bone

Text pages: 36; **Figures:** 10; **Tables:** 6

Grant sponsorship: This research was supported by The Max Planck Society and the European Research Council Starting Grant #336301.

ABSTRACT

Objectives: Internal bone structure, both cortical and trabecular bone, remodels in response to loading and may provide important information regarding behaviour. The foot is well suited to analysis of internal bone structure because it experiences the initial substrate reaction forces, due to its proximity to the substrate. Moreover, as humans and apes differ in loading of the foot, this region is relevant to questions concerning arboreal locomotion and bipedality in the hominoid fossil record.

Materials and methods: We apply a whole-bone/epiphysis approach to analyse trabecular and cortical bone in the distal tibia and talus of *Pan troglodytes* and *Homo sapiens*. We quantify bone volume fraction (BV/TV), degree of anisotropy (DA), trabecular thickness (Tb.Th), bone surface to volume ratio (BS/BV), cortical thickness, and investigate the distribution of BV/TV and cortical thickness throughout the bone/epiphysis.

Results: We find that *Pan* has a greater BV/TV, a lower BS/BV and thicker cortices than *Homo* in both the talus and distal tibia. The trabecular structure of the talus is more divergent than the tibia, having thicker, less uniformly aligned trabeculae in *Pan* compared to *Homo*. Differences in dorsiflexion at the talocrural joint and in degree of mobility at the talonavicular joint are reflected in the distribution of cortical and trabecular bone.

Discussion: Overall, quantified trabecular parameters represent overall differences in bone strength between the two species, however, DA may be directly related to joint loading. Cortical and trabecular bone distributions correlate with habitual joint positions adopted by each species, and thus have potential for interpreting joint position in fossil hominoids.

1. INTRODUCTION

Aspects of the external bony morphology of the talus and distal tibia reflect kinematic differences between how terrestrial bipedal humans and arboreal, quadrupedal African apes load their foot and ankle during locomotion (e.g. Lewis, 1980a,b,c; Stern and Susman, 1983; Latimer et al., 1987; DeSilva, 2009; Barak et al., 2013b). These morphological differences can be related to fundamental differences in foot posture: the degree of dorsiflexion at the ankle, use of the foot in an inverted position, the general conformation of the leg, and the presence of medial and longitudinal arches of the foot. For example, compared with African apes, humans have been described as having a less mediolaterally expanded anterior distal articular surface of the tibia (Latimer et al., 1987; DeSilva, 2009), an angle close to 90 degrees between the long axis and distal articular surface of the tibia (Latimer et al., 1987; DeSilva, 2009), a more symmetric talar trochlea (Latimer et al., 1987; DeSilva, 2009), a relatively stiff mid-foot without a mid-tarsal break (Elftman and Manter, 1935; DeSilva, 2010), and a complex of features, including the medial longitudinal arch, metatarsophalangeal joints and various soft tissues, which contribute to the windlass mechanism (Griffin et al., 2015) that improves locomotor efficiency (Ker et al., 1987).

In part due to the mosaic nature of fossil hominin morphology, but also due to reliance on fragmentary or isolated postcranial elements, palaeoanthropologists often differ in their interpretations of the functional significance of various morphological features. It remains unclear, based on the morphology of the ankle, whether early hominins continued to engage in a significant amount of arboreal behaviour and whether hominin species used kinematically similar or distinct forms of bipedalism, perhaps unlike the modern human bipedal gait (e.g. Day and Wood, 1968; Lisowski et al., 1974; Lisowski et al., 1976; Oxnard and Lisowski, 1980; Stern and Susman, 1983; Latimer et al., 1987; Clarke and Tobias, 1995; Harcourt-Smith and Aiello, 2004; DeSilva, 2009; DeSilva and Throckmorton, 2010; Zipfel et al., 2011; Haile-Selassie et al., 2012; DeSilva et al., 2013; Harcourt-Smith et al., 2015; Prang, 2015, 2016). Functional interpretation of the external skeletal morphology of the foot is further complicated by the role of soft tissues in limiting

or enabling adoption of different foot postures (Venkataraman, 2013a,b) and by the substantial individual variability in the flexibility of the modern human foot (Bates et al., 2013; DeSilva et al., 2015). As the foot comprises a complex system of bones, tendons, ligaments and muscles, there are potentially many different ways for it to adapt to different functions, other than by modification of external bone shape (Crompton, 2015). Even modern humans are able to access numerous resources efficiently from the arboreal environment (Kraft et al., 2014), without any apparent external morphological signal on the talus and distal tibia (Venkataraman et al., 2013a).

Analysis of internal bone structure, both cortical and trabecular bone, of the talocrural and talonavicular joint has potential to provide further insight into interpreting use of the foot in the past. While external articular morphology indicates the joint positions a species was *able* to adopt, the internal bone structure can provide information about how a joint was *actually* loaded (Ruff and Runestad, 1992; Kivell, 2016). This is because both trabecular and cortical bone structure can adapt to loading during an individual's lifetime (e.g. Lanyon, 1974; Robling et al., 2002; Pontzer et al., 2006; Ruff et al., 2006; Barak et al., 2011; Kivell, 2016), by remodelling in response to strain (Ehrlich and Lanyon, 2002). Structural adaptations can occur at the level of individual trabeculae (Schulte et al., 2013; Cresswell et al., 2015). As these individual trabeculae appear able to adapt to accommodate regional strains, it is likely that regional architectural parameters can provide information about how different areas of a joint are loaded. For example, trabecular and cortical bone distribution close to the articular surface, radiodensity patterns, and indicators of bone remodelling, correspond with predicted locations of peak loading associated with specific joint positions (Patel and Carlson, 2007; Polk et al., 2008, 2010; Mazurier et al., 2010; Zeininger et al., 2011; Carlson et al., 2013; Tsegai et al., 2013; Skinner et al., 2015).

Experimentally changing the loading regime of a joint or limb by, for example, changing the angle of the joint during loading or subjecting a limb to an unnatural load, leads to predictable alterations in both cortical and trabecular bone (Robling et al., 2002; Pontzer et al., 2006; Barak et al., 2011; Cresswell et al., 2015). It is often difficult to relate bone structure, especially that of trabecular bone, directly to the

biomechanical environment, i.e. to connect specific architectural variables to joint function and loading regime. Factors other than behaviour have the potential to influence, or even be the main factor determining, bone form (Bertram and Swartz, 1991; Lovejoy et al., 2003; Ruff et al., 2006; Kivell, 2016). There is still much that we do not fully understand about bone functional adaptation, including the genetic and systemic factors that shape trabecular and cortical structure (Lieberman, 1996; Carlson et al., 2008; Havill et al., 2010; Wallace et al., 2010; Paternoster et al., 2013; Wallace et al., 2013; Tsegai et al., 2016a). These include the way in which bone remodels depending upon the duration, frequency, or magnitude of the external load (e.g. Frost, 1987; Rubin and Lanyon, 1985; Skerry and Lanyon, 1995), or how these factors might vary depending on species (e.g. Turner, 2001), anatomical region (e.g. Morgan and Keaveny, 2001), age (e.g. Pearson and Lieberman, 2004) or body mass (e.g. Biewener, 1990; Doube et al., 2011). Moreover, cortical and trabecular bone may respond differently to strain or even interact to compensate for each other (Carlson and Judex, 2007). It is likely that these factors vary between even closely related species/subspecies. For example, some of the genetic differences between modern humans and Neanderthals relate to bone growth (Green et al., 2010), and changes in indirect measures of hormone levels occur at different developmental stages in humans, chimpanzees and bonobos (e.g. TT3: Behringer et al., 2014a; testosterone: Behringer et al., 2014b). All of these factors can confound our functional interpretations of variation in bone structure. However, there is a wealth of comparative, computational and *in vivo* research that makes clear that variation in cortical and trabecular structure reflects, at least to some degree, variation in external loading (Ruff et al., 2006; Kivell, 2016).

The hominoid foot and ankle, specifically the talocrural and talonavicular joints, are well suited to analysis of internal bone structure due to differences in foot postures adopted by modern humans and extant apes, the specific structure of the joint, and the close association of the foot with the substrate. Several studies have investigated the kinematics of the foot, during both quadrupedal and bipedal locomotion, in humans and chimpanzees (e.g. Sockol et al., 2007; Pontzer et al., 2009; Pontzer et al., 2014; O'Neill et al., 2015; Holowka et al., 2017). As modern human bipeds and chimpanzee

129 climbers/knuckle-walkers adopt divergent foot postures (DeSilva, 2009), the loading environment within
130 the foot and at the ankle is likely to differ between these groups. In *Pan troglodytes*, the ankle is loaded in
131 dorsiflexion during both vertical climbing and during quadrupedal knuckle-walking (Sockol et al., 2007;
132 DeSilva, 2009; Pontzer et al., 2009; Barak et al., 2013b; Pontzer et al., 2014), whereas the human ankle
133 adopts a more neutral posture during bipedalism (Barak et al., 2013b). The chimpanzee ankle is also
134 inverted during climbing (Lewis 1980a; Latimer et al., 1987; DeSilva, 2009). Loading at the talonavicular
135 joint is characterised by greater mobility in *Pan* compared to *Homo,* either related to dorsiflexion (i.e. the
136 midtarsal break) or to rotation (Elftman and Manter, 1935; DeSilva, 2010; Thompson et al., 2014; but see
137 Holowka et al., 2017). The high joint congruity between the distal tibia and the trochlea surface of the
138 talus (Latimer et al., 1987) indicates that the bone structure is likely to be directly related to joint use, and
139 not to other factors such as the action of muscles, as in other regions (e.g. the humeral head), where the
140 bony articulation itself does not maintain joint integrity. In the absence of muscle/tendon attachments on
141 the talus itself, and thus of tensile forces caused by muscle contractions, this region also offers an
142 opportunity to analyse the effects of locomotor forces alone on trabecular bone structure (DeSilva and
143 Devlin, 2012). Further, as the foot is in direct contact with the substrate, it directly experiences the initial
144 forces of locomotion, unlike more proximally located joints. The same is true for the hand, where clear
145 trabecular signals of the direction of loading are present (Tsegai et al., 2013; Skinner et al., 2015).

146 Previous analyses have assessed the functional significance of trabecular and cortical bone structure of the
147 ankle in humans (talus: Takechi et al., 1982; Sinha, 1985; Pal and Routal, 1998; Ebraheim et al., 1999;
148 Schiff et al., 2007; Athavale et al., 2008; Nowakowski et al., 2013; talus and distal tibia: Hvid et al.,
149 1985), and several studies have adopted a comparative approach across different taxa (talus: Su, 2011;
150 DeSilva and Devlin, 2012; Hérbert et al., 2012; Su et al., 2013; Su and Carlson, 2017; tibia: Su, 2011;
151 Barak et al., 2013b; Carlson et al., 2016). DeSilva and Devlin (2012) found interspecific differences in
152 regional patterning of trabecular structure across four quadrants of the talar body, but were unable to
153 attribute these differences to locomotor mode and a biomechanical explanation remains unclear. Analysis

of more localised subregions, sampling bone directly adjacent to the articular surface, has shown regional patterning of degree of anisotropy (DA), elongation and primary trabecular orientation, which is distinct in modern humans when compared with extant apes, with fossil hominins displaying some ape-like and some human-like features (Su, 2011; Su et al., 2013; Su andCarlson, 2017). At the distal tibia, the orientation of trabecular bone in humans and chimpanzees corresponds with measurements of dorsiflexion at the ankle (Barak et al., 2013b). Previous studies have assessed cortical thickness and radiodensity patterns of the articular surfaces of the primate talus and distal tibia (talus: Su, 2011; tibia: Su, 2011; Carlson et al., 2016), and behavioural correlates have been identified from bone profiles and radiodensity patterns at articular surfaces of other primate and mammalian taxa and epiphyses (Patel and Carlson, 2007; Mazurier et al., 2010; Carlson et al., 2013). However, to our knowledge no previous study has comparatively analysed cortical thickness maps in both the talus and distal tibia of humans and chimpanzees.

Previous studies quantifying trabecular bone structure and/or bone strength characteristics at the ankle relied on analyses of multiple volumes of interest (Su, 2011; DeSilva and Devlin, 2012; Su et al., 2013) or on destructive methods (Sinha, 1985; Athavale et al., 2008). Interspecific analyses are often complicated by the difficulty in identifying biologically homologous regions, and differences in VOI size and location have a substantial impact on trabecular bone analysis, especially when comparing among species that vary greatly in size and in morphologically complex bones (Maga et al., 2006; Kivell et al., 2011; Lazenby et al., 2011). Moreover, trabecular bone close to the articular surface, which can be difficult to sample using VOI-based methods that require manual discrimination between cortical and trabecular bone, is more likely to be of biomechanical relevance as it experiences the initial joint reaction forces, and bone closer to the articular surface differs from that in the center of the epiphysis (Singh, 1978). Analyses of bone strength at the articular surface have not investigated the cortical and trabecular structure independently, but have instead used methods which quantify cortical bone and some of the underlying trabeculae (Patel and Carlson, 2007; Mazurier et al., 2010). In this study, we address some of these

challenges by using two methodologies that allow independent quantification of the trabecular and the cortical structure. The trabecular bone analysis applied here enables quantification of trabecular structure throughout the bone or in a pre-defined region of the epiphysis, however, statistical comparisons cannot be conducted between groups. For cortical bone, we use a method that is able to compare cortical thickness across the bone/epiphysis between groups, but does not allow quantification of trabecular structure further than around 5mm beneath the cortex. By combining these complementary methodologies, we are able to analyse patterns of both cortical and trabecular bone in the human and chimpanzee talus and distal tibia. As a result, we are able to generate a fine scale, nuanced analysis through the visualisation of regional patterning of both cortical and trabecular bone, which may provide detailed information about joint loading.

In this study, we measure trabecular and cortical bone of the talus and distal tibia in *Pan troglodytes verus* and *Homo sapiens*. We test the following predictions in how trabecular bone structure and distribution, and cortical thickness and distribution differ between *Pan* and *Homo*. First, as both the talocrural and talonavicular joint are used in a greater range of positions in *Pan*, and both joints are less mobile in *Homo*, we predict a higher DA in humans in both the talus and tibia (Barak et al., 2013b; Su, 2011; Su et al., 2013; Thompson et al., 2014; Su and Carlson, 2017; but see Holowka et al., 2017). Second, following the findings of previous trabecular studies that sedentary modern humans have a generally low BV/TV and cortical thickness (Ruff et al., 1993; Lieberman, 1996; Ruff, 2005; Chirchir et al., 2015; Ryan and Shaw, 2015; Scherf et al., 2015; Chirchir et al., 2017), we predict an overall lower BV/TV and thinner cortex in *Homo.* Third, we hypothesise that the regional distribution of both cortical and trabecular bone will reflect differences in habitual peak loading of the talocrural and talonavicular joints. More specifically, that at the talocrural joint *Pan* will show a pattern of BV/TV and cortical thickness that reflects use of the foot in dorsiflexion and inversion, and at the talonavicular joint a greater degree of mobility. In *Homo*, the trabecular bone distribution and cortical thickness will reflect less mobility, and a more neutral ankle position.

2. MATERIALS AND METHODS

2.1 Sample

This study analysed trabecular and cortical bone morphology of the tibia and talus of two species with divergent modes of locomotion: *Pan troglodytes verus* and *Homo sapiens*. The sample, detailed in Table 1, included fifteen wild *P. t. verus* individuals (tibiae: N = 10; tali: N = 13; of which N = 8 were paired) whose skeletal remains were collected from the Taï National Park, Cote d'Ivoire, and ten *H. sapiens* individuals (tibia: N = 8; tali: N = 9; of which N = 7 were paired) from an 18^{th} - 19^{th} century cemetery in Inden, Germany. Adult specimens were used, based on fusion of the epiphyses throughout the skeleton and no external signs of pathology or senescence related changes were present. The right side was chosen where both talus and tibia were available and free from damage, otherwise the left side was used.

2.2 Computed tomography

High resolution micro-computed tomography (CT) scans were collected with a BIR ACTIS 225/300 CT scanner for the tibiae and with a SkyScan1173 CT scanner for the tali, using an acceleration voltage of 130kV and 100µA and either a 0.5mm brass or 1mm aluminium filter, at the Department of Human Evolution, Max Planck Institute for Evolutionary Anthropology (Leipzig, Germany). Isotropic acquisition voxel sizes were 25-36 microns for the tibia and talus of *Homo* and 19-30 microns for the tibia and talus of *Pan*. Each scan was reconstructed as a 2048 x 2048 16-bit TIFF image stack from 2500 projections with three-frame averaging. Following reconstruction, all specimens were reoriented into standardised positions using AVIZO 6.3® (Visualization Sciences Group, SAS) and segmented using a Ray Casting Algorithm (Scherf and Tilgner, 2009).

Prior to segmentation, all *Pan* specimens were resampled to 35 microns and all *Homo* specimens to 40 microns, due to processing constraints. The relative resolutions, a measure of how adequately the average trabecular strut is represented (i.e. mean trabecular thickness [mm] / resolution [mm]), are shown in Table 1. The average for the entire sample of 7.57 (range: 5.46 – 11.59) is consistent with previous studies of

trabecular bone structure (Sode et al., 2008; Kivell et al., 2011; Tsegai et al., 2013), and is appropriate for microstructural analysis.

2.3 Analysis of trabecular bone microstructure

To quantify trabecular bone, each material in the scan (Fig. 1a), i.e. cortical bone, trabecular bone, air and the internal bone cavity, were segmented automatically using an in house script in medtool v3.9 (www.dr-pahr.at), following Gross et al. (2014). Morphological filters were used to separate these regions, and the kernel size used was adjusted for each individual according to its measured trabecular thickness, enabling an accurate, subject-specific segmentation. This resulted in three data sets that were used in subsequent processing steps: (1) the trabecular bone (Fig. 1b), (2) the inner region of the bone and, (3) the inner mask (Fig. 1c), which contains the internal region of the bone where internal bone cavity and trabecular bone are represented by different grey values and the cortex has been removed. This automated segmentation was problematic in two locations in the talus, at the inferior talar neck and at the subtalar joint surfaces, due to their complex morphology. Thus the results from these regions are treated with caution. The proximal boundary of the distal tibia was defined as the point at which curvature of the shaft begins in both medial and anterior views, which is at the proximal extent of the fibular notch, and is an equivalent location across the sample.

From the trabecular only mask (Fig. 1b), trabecular thickness (Tb.Th), bone surface area (BS), and bone volume (BV) were quantified using the BoneJ plugin (version 1.3.12; Doube et al., 2010) for ImageJ v1.46r (Schneider et al., 2012). Bone surface to volume ratio (BS/BV) was subsequently calculated.

The inner region of the bone was used to create a 3D tetrahedral mesh with a mesh size of 1mm, using CGAL 4.4 (CGAL, Computational Geometry, http://www.cgal.org). The inner mask (Fig. 1c) was used to calculate BV/TV throughout the bone to generate 3D colour maps of bone distribution, and to calculate the overall bone volume fraction (BV/TV) and degree of anisotropy (DA) using medtool v3.9. A rectangular background grid, with a grid size of 2.5mm, was applied and a spherical VOI with a diameter

of 5mm was used to measure BV/TV at each node of the grid. A sphere size of 5mm is appropriate as enough trabecular struts are sampled to adequately quantify trabecular parameters (Gross et al., 2014). To create a 3D colour map of bone distribution, the BV/TV values at each node were interpolated to assign each element in the 3D mesh of the trabecular region a BV/TV value (Fig. 1d). The colour maps were visualized in Paraview v4.0.1 (Ahrens et al., 2005). The overall BV/TV value was calculated as the mean of the values for each element in the 3D mesh, and thus is the average for the whole bone/epiphysis. The mean intercept method (Whitehouse, 1974; Odgaard, 1997) was used to calculate the mean fabric tensor, the arithmetic mean of all second order fabric tensors normalised using the determinants. The extracted eigenvalues and eigenvectors were then used to calculate the DA (DA = 1 – [smallest eigenvalue/largest eigenvalue]), whereby a DA of 1 indicates complete anisotropy and a DA of 0 complete isotropy.

2.4 Analysis of cortical bone microstructure

To compare cortical thickness between *Pan* and *Homo* in the talus and distal tibia, cortical bone thickness maps were generated for each specimen (following Treece et al., 2010; Treece et al., 2012; Tsegai et al., 2016b). This was accomplished via semi-automatic segmentation of the cortical surface, from the unsegmented CT data (Fig. 1e-f) in Stradwin v5.1a (Treece, Gee, Cambridge; http://mi.eng.cam.ac.uk/~rwp/stradwin). Following definition of the surface, around 15,000 independent measurements of cortical thickness were calculated throughout the bone (Fig. 1f) and mapped onto a subject specific surface (Fig. 1g). Subsequently, each surface was registered to a canonical surface using wxRegSurf v13 (Fig. 1h). The canonical surface used was an average of the entire sample, each species was averaged separately and then the average of the two resulting surfaces was used, to prevent the difference in sample size affecting the average morphology. After registration to the canonical surface, mean thickness maps were generated for each species.

2.5 Statistical analysis

For trabecular bone analysis, all statistical tests were performed using R v3.0.3 (R Core Team, 2016) and ggplot2 was used for generating plots (Wickham, 2009). Shapiro-Wilk test for normality showed that the

data were not normally distributed and thus non-parametric tests were used. Mann-Whitney U tests were used to test for statistical differences in trabecular bone parameters between *Homo* and *Pan*. A principal component analysis was conducted to determine which parameters contributed to interspecific differences in the talus and in the tibia. All variables were included in the principal component analysis: Tb.Th, BV/TV, DA, BS/BV, and cortical thickness. As there are large differences in the variances of these variables, prior to analysis the data was centered and scaled to unit variance. Principal components were subsequently derived by singular value decomposition of the resulting data matrix. Spearman's correlation test and RMA regression were used to test for correlation between trabecular parameters and cortical thickness in the talus and distal tibia. To test the relationship between size and trabecular bone parameters, OLS $\log_{10}$ regressions and Pearson's correlation tests were conducted for each trabecular parameter against the size of the epiphysis/bone for each taxon. The size of each bone was represented as the geometric mean of several measurements, both of overall bone size and of the size of the articular surfaces. For the talus, these measurements were the anteroposterior length, mediolateral width and dorsoplantar height of the talus, the anteroposterior length and mediolateral width of the talar trochlea, and the dorsoplantar height and mediolateral width of the talar head. For the tibia, a geometric mean was derived from the maximum anteroposterior length and maximum mediolateral width of the distal tibia, the anteroposterior length and mediolateral width of the distal articular surface, the anteroposterior length, mediolateral width and proximodistal height of the medial malleolus. Pearson's correlation test was used to compare trabecular parameters between paired tibia and tali in each taxon. Statistical parametric mapping was used to identify regional cortical thickness differences between the two species (Friston et al., 1995), using the SurfStat package (Worsley et al., 2009), by fitting a general linear model (GLM) to the data. This model determined whether cortical thickness differences could be explained by species (covariates of interest) or other factors (confounding covariates). As there is risk of systematic misregistration due to shape differences, non-rigid shape coefficients were included as confounds in the GLM (Gee and Treece, 2014; Gee et al., 2015). Bone size, however, was strongly correlated with species and therefore not included as a confound in the GLM. Statistical parametric maps were generated using F

303 statistics and the corresponding p-values were corrected for multiple comparisons using random field
304 theory to control for the chance of false positives. Relative cortical thickness was calculated for each
305 specimen, by subtracting the individual mean value from each individual thickness measurement and
306 dividing by the standard deviation. In this way, relative patterns of cortical thickness could be analysed,
307 despite considerable interspecific differences in absolute cortical thickness. For all statistical tests, a *p*
308 value of <0.05 was considered significant.

309 # 3 RESULTS

310 ## 3.1 Trabecular and cortical architecture of the talus and tibia

311 Means and standard deviations of measured trabecular and cortical parameters and Mann-Whitney U test
312 results are shown in Table 2, and extracted regions of trabecular bone, visualizing structural differences,
313 are shown in Figure 2. Mann-Whitney U test results (Table 2) find that the trabecular structure of *Pan*
314 differs from that of *Homo* in having a significantly greater BV/TV and lower BS/BV in both the talus and
315 the tibia. The trabecular structure is more divergent in the talus than in the tibia: with the talus of *Pan*
316 having significantly thicker, less uniformly-oriented trabeculae (i.e. lower DA). The cortex of *Pan* is
317 significantly thicker in both the talus and the tibia compared to *Homo*.

318 Correlations between parameters in the talus and tibia of each taxon are reported in Table 3. Significant
319 correlations between variables differ both between taxa and between skeletal regions. As such, all
320 parameters were included in the analysis, although correlations between parameters may lead to
321 overemphasis of the contribution of these variables. Table 4 shows the results of the principal component
322 (PC) analysis, and Figure 3 shows the plot of PC1 against PC2 for both the talus and tibia. Together, PC1
323 and PC2 explain 92.90% and 90.85% of the variance for the talus and tibia, respectively and in both
324 analyses, *Homo* and *Pan* are clearly separated. All four trabecular parameters and cortical thickness
325 contribute equally to PC1 in the talus, distinguishing *Pan*, with greater BV/TV, Tb.Th and cortical
326 thickness, but lower DA and BS/BV, from *Homo*. PC2 is driven by Tb.Th and BS/BV, but only separates
327 out particular individuals within each taxon. In the tibia, separation along PC1 is largely determined by

BV/TV, BS/BV and cortical thickness. Along PC2, most *Pan* individuals are distinguished from *Homo* in having lower Tb.Th and higher DA.

3.2 Allometry

The results of the $\log_{10}$ OLS regressions of each parameter against the geometric mean, a proxy for bone size, are shown for *Pan* and *Homo* in Table 5 and Figures 4 and 5. There were no significant correlations between any trabecular parameter and bone size. However, the relationship between size and trabecular and cortical structure does differ between species and between the talus and tibia (Figs. 4-5).

3.3 Correlation between the talus and tibia

Paired tali and tibiae were used to compare trabecular and cortical bone parameters between the talus and tibia in seven *Homo* and eight *Pan* specimens (Table 6 and Fig. 6). Within *Pan*, all parameters other than DA are strongly correlated across the joint (i.e. $r > 0.70$), whereas in *Homo*, only Tb.Th and BS/BV are strongly and significantly correlated.

3.4 Distribution of trabecular bone in the talus and distal tibia

Figure 7 shows BV/TV colour maps for the talus of one representative individual of *Homo* and *Pan.* Images of the full sample are included in the Supporting Information.

On the dorsal surface of the talus (Fig. 7 a and f), all *Pan* specimens share a region of high BV/TV on the lateral edge of the trochlea. In some individuals this extends posteriorly along the edge, and in others it is more anteriorly confined. Some, but not all, specimens have an additional region of higher BV/TV on the medial trochlea, which is not consistent in its location or antero-posterior extent (see Supporting Information). In *Homo*, there is no consistent pattern of trabecular bone distribution on the dorsal surface of the trochlea as this region is highly variable across the sample. All individuals of both *Pan* and *Homo* have a region of high BV/TV on the dorsal surface of the talar neck, although this is much more pronounced in *Pan*. In a transverse plane, where the superior portion of the talus has been removed (Fig. 7 b and g), there is a region of high BV/TV at the neck in *Pan*, although, as mentioned above, the inferior

region of the neck must be interpreted with a certain degree of caution due to problems segmenting trabeculae from cortex. In *Homo*, there is no localised region of high BV/TV in the neck, but instead an anteroposterior trajectory of bone running through the head and neck, which is absent in *Pan*. The region of high BV/TV at the articular surface of the talar head (i.e. at the talonavicular joint), is more localized in *Homo* than in *Pan*. This is clearly seen in anterior view (Fig. 7 c and h), where *Homo* has a point of high BV/TV located dorsally on the head, in contrast to *Pan*, where there is a band running mediolaterally across the head. In the coronal (Fig. 7 d and i) and sagittal (Fig. 7 e and k) planes of *Homo*, the centre of the talar body contains a relatively higher BV/TV than in *Pan.* Also, in the sagittal plane (Fig. 7 e and k) there is a distinct trajectory of high BV/TV running antero-posteriorly through the talar head of *Homo* that is not found in *Pan.* Instead, the *Pan* neck has a region of high BV/TV on the dorsal surface. Comparison of the individual BV/TV scales shows that *Pan* has a higher BV/TV than *Homo* in both its minimum and maximum values.

Colour maps of the BV/TV distribution in the distal tibia of *Homo* and *Pan* are shown in Figure 8 and results for the entire sample are included in the Supporting Information. On the distal articular surface of the tibia (Fig. 8a and e), some specimens of *Homo* have a high concentration of BV/TV confined to the medial side of the articular surface and in other individuals it is centrally located. This is in contrast to *Pan*, where there are consistently three regions of higher BV/TV: anterolateral, anteromedial and posterocentral. When viewed in the mid-sagittal plane of the distal tibia (Fig. 8 b and f), the anteromedial and posterior concentrations of bone are visible in *Pan,* in contrast to the more central and continuous area of high BV/TV in *Homo*. On the anterior edge of the distal tibia (Fig. 8 c and g), *Pan* has a high concentration of bone extending across the edge that is absent in *Homo*. In the mid-coronal plane (Fig. 8 d and h), *Pan* contains a relatively greater BV/TV in the centre of the medial malleolus, compared to *Homo*. Unlike the talus, the range of BV/TV is more similar between the two species (Fig 7 and Fig 8, scale bars).

3.5 Distribution of cortical bone in the talus and distal tibia

Mean relative cortical thickness maps for the talus and distal tibia of *Pan* and *Homo*, along with regions of significant differences, are shown in Figures 9 and 10. In contrast to the trabecular bone maps, these figures do not show the cortical thickness in just one individual, but rather the mean of all individuals by taxon. As *Pan* has a greater cortical thickness in both the talus and the distal tibia, results are presented for relative cortical thickness values, equalized by subtracting the mean value from each cortical thickness value and dividing by the standard deviation for every individual in the sample.

Visual comparison between the relative cortical thickness maps of the talus in *Homo* (Fig. 9a) and *Pan* (Fig. 9b), show that the regions of thickest cortical bone differ between the two species. On the talar head, *Homo* has a dorsally located region of highest relative thickness, whereas in *Pan* the region of high thickness runs mediolaterally along the dorsal half of the articular surface. At the trochlea, *Pan* has a higher cortical thickness on the lateral edge, whereas in *Homo* it is the centromedial region that has the highest mean thickness. *Pan* and *Homo* share thick cortical bone around the region of the talar neck, however, in *Pan* this extends around the entire dorsal region of the neck, whereas in *Homo* it is confined to the dorso-lateral side. In *Homo* the centre of the posterior subtalar articular surface has the thickest cortical bone, whereas in *Pan* the cortical bone is thickest anterolaterally on this articular surface. Differences between *Pan* and *Homo* are shown in Figure 9c, and regions where these differences reach significance are shown in Figure 9d. There are several regions with significant differences located at the articular surfaces of the talus. *Pan* has relatively thinner bone compared to *Homo* on the anterior surface of the talar head, on the anteromedial region of the talar trochlea and on the dorsal edge of the talar head, and relatively thicker bone compared to *Homo* in a band anterolaterally on the posterior subtalar articular surface.

Cortical thickness maps, showing relative cortical thickness are shown for *Homo* and *Pan* in Figure 10a and b, respectively. In distal view, *Homo* has thickest cortical bone the along the medial edge of the distal articular surface and the distal end of the medial malleolus. Both taxa share regions of thicker cortical bone on the distal end of the medial malleolus and the medial edge of the distal articular surface. This

region on the medial articular surface is relatively thicker anteriorly in *Pan*, whereas in *Homo* this feature extends along the medial border of the articular surface. *Pan* has two additional regions of thicker cortical bone on the anterolateral and posterocentral regions of the distal articular surface. Comparisons of relative cortical thickness values between *Homo* and *Pan* are shown in Figure 10c and regions with significant differences are shown in Figure 10d. At the distal articular surfaces, *Pan* has significantly thicker cortex at the anteromedial corner, extending along the anteromedial edge of the medial malleolus. There is significantly thicker cortical bone on the distal surface of the medial malleolus in *Pan* compared to *Homo*.

4 DISCUSSION

We analysed the internal bone structure of the talus and distal tibia in bipedal *Homo* and arboreal, quadrupedal *Pan*. We find that trabecular and cortical bone, both the measured parameters and the regional distribution of bone, differed, often significantly, between the two taxa in ways that are potentially related to variation in joint position and load distribution during locomotion. In addition to these differences, we find further support for previously proposed systemically weaker trabecular and cortical bone in recent humans (Ruff et al., 1993; Lieberman, 1996; Ruff, 2005; Chirchir et al., 2015; Ryan and Shaw, 2015; Scherf et al., 2015; Chichir et al., 2017).

4.1 Identifying functional signals in internal bone structure

The relationship between bone form and mechanical loading is complex. It may be influenced by numerous factors that affect bone growth and structure, which are likely to differ systematically between species and, as such, bone structure should be considered within the broader context of what is already known about the bone architecture of each species. In both the talus and distal tibia of *Homo*, we find support for our prediction that bone is relatively weak, having a lower BV/TV, a higher BS/BV and thinner cortices, compared with the more robust *Pan*. BV/TV is the strongest predictor of trabecular bone stiffness, or Young's modulus; it alone explains 87-89% of variance in stiffness (Stauber et al., 2006; Maquer et al., 2015). Cortical bone thickness is also related to bone strength, as thin cortices are associated with increased fracture risk (Augat and Schorlemmer, 2006). The difference in trabecular

BV/TV and cortical thickness between *Pan* and *Homo* is consistent with previous findings for the talus and distal tibia (talus: Su, 2011; DeSilva and Devlin, 2012; Su and Carlson, 2017; tibia: Su, 2011; Barak et al., 2013b), and with the trabecular morphology of other anatomical regions (e.g. third metacarpal: Tsegai et al., 2013; calcaneus: Maga et al., 2006; Zeininger et al., 2016; first and second metatarsal: Griffin et al., 2010; systemic: Chirchir et al., 2015). As the biomechanical environment of different joints in the human and chimpanzee are likely to vary given their divergent modes of locomotion, this consistent difference across several anatomical sites may be part of a systemic pattern (i.e. in all regions of the skeleton) and not due to specific locomotor, or other, behaviour. This gracility of the modern human skeleton may be associated with increased sedentism following the adoption of agriculture, as early hominins and recent hunter gatherers/foragers have a more robust skeleton (Ruff et al., 1993; Lieberman, 1996; Ruff, 2005; Chirchir et al., 2015; Ryan and Shaw, 2015; Scherf et al., 2015). Analysis of the relationship between these structural parameters and size are limited by small sample sizes.

There are aspects of bone structure that appear likely to reflect joint function and thus can be of use for reconstructing behaviour in the fossil record. Here, we find support for our prediction that the human talus has a significantly higher DA than in *Pan*. However, contrary to our predictions, we find no significant difference for the distal tibia. During human bipedalism the mid-foot forms a relatively rigid lever during push off (Morris, 1977), compared with the flexibility of the chimpanzee mid-foot (Elftman and Manter, 1935; Susman, 1983; Thompson et al., 2014; but see Holowka et al., 2017). There is also less mobility at the ankle of *Homo* than in *Pan* (Latimer et al., 1987). The less aligned trabeculae of the *Pan* talus are consistent with being more able to withstand forces from multiple directions associated with a wider range of joint positions, whereas the more highly aligned trabecular structure of the *Homo* talus appears to reflect more stereotypical loading (Su, 2011; DeSilva and Devlin, 2012; Su et al., 2013; Su and Carlson, 2017). In contrast to previous studies (Su, 2011; Barak et al., 2013b), we do not find a higher DA in the distal tibia of *Homo*, but rather higher (although not significantly so) mean DA in *Pan*. However, Su (2011) found that trabeculae in *Homo* were significantly more uniformly aligned in the talus compared

with the tibia, suggesting that more similar DA values in the *Homo* and *Pan* distal tibia are not unexpected.

DA may hold a functional signal for different types of behaviour that engender more or less stereotypical loads at a joint. Regional differences in DA have been useful in distinguishing between primate locomotor groups, with the structure of the proximal femur being consistent with inferred differences in loading in leaping and slow climbing strepsirrhines (Ryan and Ketcham, 2002a,b; MacLatchy and Muller, 2002; Ketcham and Ryan, 2004). The trabecular structure of the human foot is generally more highly aligned than other apes (first and second metatarsal: Griffin et al., 2010; calcaneus: Maga et al., 2006; Zeininger et al., 2016; but see Kuo et al., 2013; talus: Su, 2011; Su et al., 2013; Su and Carlson, 2017). It seems unlikely that this would relate to differences in activity level between the taxa, and there are no consistent differences in DA in the proximal femur (Ryan and Shaw, 2015) or humerus (Scherf et al., 2015) between human populations with different activity levels (i.e. engaging in the same behaviours but at different frequencies). Adult trabecular structure could reflect individual or interspecific differences in loading during puberty, at a time when bone is more responsive to strain (e.g. Pettersson et al. 2010; for cortical bone see Pearson and Lieberman, 2004). However, homologous regions of trabecular bone in adolescent and adult humans have not been sampled, as many studies exploring ontogeny have investigated changes in structure between non-adult groups (Ryan and Krovitz, 2006; Ryan et al., 2007; Gosman and Ketcham, 2009; Raichlen et al., 2015). DA in the proximal tibial metaphysis and in the ilium continue to change between adolescence and adulthood (Gosman & Ketcham, 2009; Abel & Macho, 2011). Moreover, chimpanzees reach adult-like locomotor behaviour by adolescence (Doran, 1992; Sarringhaus et al., 2014), while humans reach this point during early childhood (e.g. Sutherland et al., 1980; Beck et al., 1981; Raichlen et al., 2015). Trabecular orientation in the talus also shows plasticity later in life, as degeneration of articular cartilage, i.e. changes at the joint surface that affect loading, is associated with differences in trabecular orientation in humans (Schiff et al., 2007). This indicates that DA in adult humans and chimpanzees is likely to reflect adult behaviour patterns, as loading from locomotion has

remained generally consistent during much of the later growth period. Together these results suggest that the high degree of trabecular alignment throughout several elements of the human foot may be a behavioural signal related to the stereotypical loading of terrestrial bipedality. We suggest that, using our methodology, DA may provide functional information about loading in the talus, but not the tibia.

4.2 The relationship between joint position and bone distribution

We predicted that differences in the cortical and trabecular bone distribution maps would reflect variation in dorsiflexion and inversion of the talocrural joint and the degree of mobility at the talonavicular joint. The colour maps of cortical and trabecular bone support some, but not all, of these predictions. These results are based on mean cortical thickness distribution maps and significant differences, and on BV/TV distribution maps for each individual. Generation of mean morphometric maps for BV/TV was not conducted due to the complexity of registering 3D meshes while ensuring homology.

4.2.1 Dorsiflexion

Dorsiflexion at the ankle is characteristic of both climbing and knuckle-walking in chimpanzees compared to the more neutral ankle posture adopted by humans during bipedalism. We find no clear signal of dorsiflexion in trabecular and cortical bone of the talar trochlea, but are able to identify differences in internal bone structure of the distal tibia that we propose are related to degree of dorsiflexion. In chimpanzees, during knuckle-walking the angle between the long axis of the tibia and the foot is 75.2 degrees, compared with 85.6 degrees in normal human bipedalism (Barak et al., 2013b). During vertical climbing the degree of dorsiflexion is much greater, with an angle between the long axis of the tibia and the foot of 44.5 degrees (DeSilva, 2009). The external morphology of the talar trochlea and the distal articular surface of the tibia is associated with this difference in loading of the ankle (DeSilva, 2009; but see Venkataraman et al., 2013a). It might be expected that the distribution of trabecular bone and cortical bone in the talar trochlea of *Pan* would be more anteriorly distributed, reflecting this difference in joint angle. However, we find no clear signal across the study sample in either the trabecular or cortical bone distribution maps. This is consistent with previous studies that did not

identify differences in BV/TV across quadrants of the talar body (DeSilva and Devlin, 2012), or higher BV/TV and cortical thickness in the anterior talar trochlea (Su, 2011; Su and Carlson, 2017).

In contrast to the talus, we did find that the trabecular and cortical bone structure of the distal tibia reflected the differences in joint position between *Homo* and *Pan*. *Pan* shows two regions of higher BV/TV and thicker cortical bone, located at the anterior portion of the distal articular surface of the tibia, one lateral and one medial. In addition, the anterior edge of the distal articular surface has a higher BV/TV, which extends up anteriorly through the epiphysis. This is in contrast to *Homo*, where BV/TV maps show a more central concentration of trabecular bone. In *Homo*, the cortex is thickest on the medial edge of the articular surface, adjacent to the medial malleolus. In several (but not all) individuals in the study sample (see Supporting Information), this medial region also has a high BV/TV. Although direct comparison between results from different subregions is complex, some of these findings are supported by the results of Su (2011). Fewer significant differences in BV/TV and cortical thickness are found across the *Homo* tibia compared to *Pan*, and *Pan* has generally higher BV/TV anteriorly and posteriorly. This is not the case for cortical thickness, where both *Homo* and *Pan* have thicker bone on the antero- and postero- medial regions, and in *Pan*, the posterocentral region of the articular surface (Su, 2011). Perhaps also relevant to the degree of flexion at the ankle, there is a region of high BV/TV and cortical thickness posterocentrally on the distal articular surface in *Pan*, with the region of high BV/TV extending into the bone. This could indicate increased loading during plantarflexion in *Pan* compared to *Homo*, however, this is not supported by kinematic data. Previous findings in the distal tibia of *Pan* also found that the posterior region has a higher BV/TV than the central region, and thicker cortical bone was found in the posterocentral region (Su, 2011; Su and Carlson, 2017).

In the absence of detailed kinematic data on joint contact areas, in particular for *Pan* (for humans see Wan et al., 2006; Bae et al., 2015), our understanding of the differences in the loading of the trochlea in these two species is limited. Moreover, we must make assumptions about which aspects of a species' locomotor, or other, behaviour contribute most to the remodelling of bone. Previous studies in humans

have identified areas of contact and distribution of pressure on the talus using a finite element simulation of the human foot during walking (Bae et al., 2015) and on both the talar trochlear and distal articular surface of the tibia under pressure using dual orthogonal fluoroscopy (Wan et al., 2006; Caputo et al., 2009; Bischof et al., 2010). During human bipedalism, ground reaction forces (GRF) peak at two phases, first after heelstrike and before midstance, and second at toe off (Bae et al., 2015; Alexander, 2004), with contact pressure and strain increasing throughout the stride, peaking at toe off (Bae et al., 2015). After heelstrike, during the first peak in GRF, there is contact between the cartilage of the talus and tibia on the latero-central trochlea (Wan et al., 2006; Bae et al., 2015). During stride, the area of contact moves anteriorly (Wan et al., 2006; Bae et al., 2015) and the point of highest pressure moves anterocentrally until toe off, when both the contact area and point of highest pressure are located on the anterior of the trochlea, just lateral to the midline (Bae et al., 2015). At the distal tibia, contact is located antero-posteriorly at heel strike, moving anteriorly across the medio-lateral extent of the articular surface at mid-stance, and at heel strike in the anterolateral half of the distal articular surface of the tibia (Wan et al., 2006). Although some of the human sample in this study have a region of high BV/TV on the anterior talus, just lateral to the midline, near the location of highest pressure (Bae et al., 2015), this is not always the region of highest BV/TV, and does vary within the sample. There is also no direct correspondence between regions of contact and areas with thicker cortices. There are several potential explanations for why the trabecular and cortical bone structure of the talar trochlea does not, as expected, reflect differences in dorsiflexion at the ankle. Firstly, experimental measures of cartilage contact and pressure may not necessarily correspond to the regions experiencing the greatest forces during life. Secondly, modern humans differ greatly in their gait. For example, there is inter-individual variation in the presence of a mid-tarsal break, and intra-individual variation between strides (Bates et al., 2013; DeSilva et al., 2015). There is also variability in foot strike patterns, with individuals making initial contact with the fore-foot, midfoot or heel, that could also contribute to variability in loading of the trochlea (e.g. during running: Lieberman et al., 2010; Hatala et al., 2013). Thirdly, differences in the external morphology of the talus may accommodate the different distribution of forces, i.e. different shaped tali absorb loads

553 differently, thus cortical thickness and trabecular architecture do not directly reflect differences in joint
554 position.

555 Due to interest in adaptations of the human skeleton to bipedal locomotion, many biomechanical analyses
556 of *Pan* have focused on bipedal walking (e.g. Susman, 1983; Thorpe et al., 2004; Wang et al., 2014;
557 O'Neill et al., 2015), although several studies have investigated kinematics of knuckle-walking in
558 bonobos (e.g. Vereecke et al., 2003; D'Août et al., 2004; Schoonaert et al., 2016). Although no *in vivo*
559 measurements of joint movement or cartilage contact are available for *Pan*, there is evidence of force
560 transmission due to contact between the anterior edge of the distal tibia and the neck of the talus. This can
561 be observed when manipulating dry, associated tibia and tali, where in an extreme position of dorsiflexion
562 the ankle joint retains congruity while there is contact between the talar neck and the anterior border of
563 the tibia in African apes, but not in *Homo* (Latimer et al., 1987). Modern humans who regularly adopt
564 crouched positions develop squatting faces on the talus and tibia (Boulle, 2001). The BV/TV distribution
565 may reflect this and indicate high loads transmitted through this region. On the medial and lateral side of
566 the talar neck and on the anteroinferior border of the tibia, *Pan* has regions of high BV/TV, which are
567 absent in *Homo*. This may reflect habitual loading of these regions in an ankle dorsiflexed to such a
568 degree that force transmission occurs between the antero-inferior edge of the distal tibia and the talar
569 neck.

570 ***4.2.2 Talonavicular mobility***

571 We find a clear signal of differences in joint mobility at the talonavicular joint in the trabecular and
572 cortical bone structure. Two features in which human bipedalism is distinct from ape quadrupedalism are,
573 firstly, weight transfer from the lateral to medial side of the foot during midstance; and secondly, in
574 having a rigid mid-foot, so that the foot acts as a lever during toe off (Elftman and Manter, 1935). The
575 medial side of the midtarsal joint (the talonavicular joint) is more mobile than the lateral side
576 (calcaneocuboid and cuboid-MT5 joints), during stance phase the talus rotates, along with the leg and
577 calcaneus, creating a close packed talonavicular joint (Elftman, 1960; Siegler et al., 1988; Scott and

Winter, 1991). Although investigations of mid-foot mobility in *Pan* have largely focused on the mid-tarsal break at the lateral side (DeSilva, 2010), there is greater movement at the talonavicular joint which, during passive dorsiflexion of the foot, is characterised by rotation in the coronal plane (Thompson et al., 2014). Furthermore, there is greater inter-individual and intra-individual variability in mobility of the human lateral midfoot than was previously assumed (Elftman and Manter, 1935; Bates et al., 2013). During bipedalism, humans have greater midfoot mobility during push off, which is characterised by plantarflexion and adduction, whereas chimpanzees have higher dorsiflexion at the midfoot (mid-tarsal break) during the single limb support period (Holowka et al., 2017). Contrary to expectations, the human midfoot was found to be overall more mobile than that of chimpanzees (Holowka et al., 2017), however, precise kinematics of the talonavicular joint remain unknown.

There are clear differences between the study taxa in the trabecular bone distribution at the talar head, where *Pan* has a band of high BV/TV running mediolaterally across the talar head, and in *Homo* there is a localised point of high BV/TV. In cortical thickness, *Pan* has relatively thinner cortices at the talar head, which is significantly thinner in the central region. Previous studies have measured both trabecular bone in the medial and lateral sides of the head (DeSilva and Devlin, 2012) and trabecular bone adjacent to the neck of the talus (i.e. on the anteromedial region of the talar trochlea). When comparing the medial and lateral side of the head of the talus in humans to other species, DeSilva and Devlin (2012) found no significant difference in DA, although the trabeculae were significantly thicker in the lateral head and significantly more connected in the medial head of humans compared to other species (DeSilva and Devlin, 2012). In the anteromedial trochlea, humans have a unique orientation of trabeculae compared to other great apes, in having trabeculae with a primarily anteroinferior orientation, i.e. parallel to the talar neck; a pattern shared with an early Pleistocene biped, KNM-ER 1464 (Su, 2011; Su et al., 2013; Su and Carlson, 2017). This distinct orientation of trabeculae in bipedal species noted by Su et al. (2013) may correspond to the trajectory of bone that we show here, travelling through the talar head into the trochlea.

The trabecular and cortical distribution of the talar head reveals a clear difference in bone structure, perhaps related to differences in midfoot mobility between the study species.

4.2.3 Inversion

As well as dorsiflexion, inversion of the foot is characteristic of arboreal behaviour in *Pan*, including vertical climbing (DeSilva, 2009). Species that engage in more arboreal locomotion have a less symmetrical trochlea surface, where the lateral trochlea ridge is higher than the medial. This asymmetry increases the difference in the radius of curvature of the medial and lateral side, thereby increasing the arcuate path of the tibia over the talus (Latimer et al., 1987), a difference that has even been identified between more arboreal western and more terrestrial eastern gorillas (Dunn et al., 2014). Of potential interest with regard to identifying signals of inversion, is the high BV/TV on the anterolateral lip of the trochlea of the talus that is consistent throughout the sample of *Pan.* This region also has a slightly thicker cortex in *Pan* than in *Homo*, with *Pan* having relatively thinner cortical bone than *Homo* on the anteromedial region of the trochlea. This is consistent with previous findings of high BV/TV, but not thicker cortices, on the anterolateral two thirds of the trochlea in *Pan* (Su, 2011; Su and Carlson, 2017). This may reflect increased shearing stresses associated with adoption of inverted foot postures, which are also mitigated by having a higher lateral ridge of the talus. More detailed understanding of the kinematics of climbing and knuckle-walking, along with modelling of the forces experienced by the talus, may improve interpretation of this signal.

5 CONCLUSION

Identifying those features of internal bone structure that are directly related to joint loading is often problematic. Here, we find that average architectural variables (BV/TV, BS/BV and cortical thickness) that relate to overall bone strength differ between *Pan* and *Homo*. These may be part of a systemic pattern unrelated to joint function, but rather due to other factors such as overall activity levels, and therefore may not be relevant for reconstructing loading of individual joints. However, the degree to which

trabeculae are uniformly oriented (DA) in the talus does correspond to variation in joint loading due to different locomotor behaviours, clearly differentiating between the more stereotypical loading regime of bipedalism in *Homo* and the greater range of motion and joint loading typical of arboreal behaviours in *Pan*. In contrast to these architectural variables quantified throughout the epiphysis/bone, more precise information about locomotor behaviour can be obtained from patterns of trabecular and cortical bone distribution. The trabecular and cortical bone distribution of the distal tibia and talus reflect differences in dorsiflexion at the ankle and range of motion at the talonavicular joint in humans and chimpanzees. Thus, the distribution of both trabecular and cortical bone in the talus and distal tibia holds potential for interpreting loading regimes and reconstructing loaded joint positions in fossil specimens.

ACKNOWLEDGEMENTS

This research was supported by The Max Planck Society (ZJT, TLK, MMS and JJH) and the European Research Council Starting Grant #336301 (TLK and MMS). We thank Christophe Boesch (Max Planck Institute for Evolutionary Anthropology) and Birgit Grosskopf (University of Göttingen) for access to specimens in their care. For assistance with CT scanning we thank David Plotzki, Heiko Temming and Patrick Schönfeld. Helpful discussions with Nicholas Stephens and comments from two anonymous reviewers greatly improved this manuscript.

REFERENCES

Abel, R., & Macho, G. A. (2011). Ontogenetic changes in the internal and external morphology of the ilium in modern humans. *Journal of Anatomy*, 218, 324-335.

Ahrens, J., Geveci, B., & Law, C. (2005). ParaView: An end-user tool for large data visualization. In C. D. Hansen & C. R. Johnson (Eds.), *Visualization Handbook* (pp. 717-731). Burlington: Butterworth-Heinemann.

Alexander, R. M. (2004). Bipedal animals, and their differences from humans. *Journal of Anatomy*, 204, 321-330.

Athavale, S. A., Joshi, S. D., & Joshi S. S. (2008). Internal architecture of the talus. *Foot & Ankle International*, 29, 82-86.

653 Augat, P., & Schorlemmer, S. (2006). The role of cortical bone and its microstructure in bone strength.
654 *Age and Ageing*, 35, 27-31.

655 Bae, J. Y., Park, K. S., Seon, J. K., & Jeon, I. (2015). Analysis of the effects of normal walking on ankle
656 joint contact characteristics after acute inversion ankle sprain. *Annals of Biomedical Engineering*, 43,
657 3015-3024.

658 Barak, M. M., Lieberman, D. E., & Hublin J.-J. (2013a). Of mice, rats and men: Trabecular bone
659 architecture in mammals scales to body mass with negative allometry. *Journal of Structural Biology*, 183,
660 123-131.

661 Barak, M. M., Lieberman, D. E., Raichlen, D., Pontzer, H., Warrener, A. G., & Hublin, J.-J. (2013b).
662 Trabecular evidence for a human-like gait in *Australopithecus africanus*. *PLoS ONE*, 8, e77687.

663 Barak, M. M., Lieberman, D. E., & Hublin, J.-J. (2011). A Wolff in sheep's clothing: Trabecular bone
664 adaptation in response to changes in joint loading orientation. *Bone*, 49, 1141-1151.

665 Bates, K. T., Collins, D., Savage, R., McClymont, J., Webster, E., Pataky, T. C., . . . Crompton, R. H.
666 (2013). The evolution of compliance in the human lateral mid-foot. *Proceedings of the Royal Society B:*
667 *Biological Sciences*, 280, 20131818.

668 Beck, R. J., Andriacchi, T. P., Kuo, K. N., Fermier, R. W., & Galante, J. O. (1981). Changes in the gait
669 patterns of growing children. *Journal of Bone and Joint Surgery*, 63A, 1452-1457.

670 Behringer, V., Deschner, T., Deimel, C., Stevens, J. M. G., & Hohmann, G. (2014a). Age-related changes
671 in urinary testosterone levels suggest differences in puberty onset and divergent life history strategies in
672 bonobos and chimpanzees. *Hormones and Behavior*, 66, 525–533.

673 Behringer, V., Deschner, T., Murtagh, R., Stevens, J. M. G., & Hohmann, G. (2014b). Age-related
674 changes in thyroid hormone levels of bonobos and chimpanzees indicate heterochrony in development.
675 *Journal of Human Evolution*, 66, 83-88.

676 Bertram, J. E. A., & Swartz, S. M. (1991). The 'law of bone transformation': A case of crying Wolff?
677 *Biological Reviews*, 66, 245-273.

678 Biewener, A. A. (1990). Biomechanics of mammalian terrestrial locomotion. *Science*, 250, 1097-1103.

679 Bischof, J. E., Spritzer, C. E., Caputo, A. M., Easley, M. E., DeOrio, J. K., Nunley, J. A., & DeFrate L. E.
680 (2010). In vivo cartilage contact strains in patients with lateral ankle instability. *Journal of Biomechanics*,
681 43, 2561-2566.

682 Boulle, E.-L. (2001). Evolution of two human skeletal markers of the squatting position: A diachronic
683 study from antiquity to the modern age. *American Journal of Physical Anthropology*, 115, 50-56.

684 Caputo, A. M., Lee, J. Y., Spritzer, C. E., Easley, M. E., DeOrio, J. K., Nunley, J. A., & DeFrate, L. E.
685 (2009). In vivo kinematics of the tibiotalar joint after lateral ankle instability. *The American Journal of*
686 *Sports Medicine*, 37, 2241-2248.

687 Carlson, K. J., Chirchir, H., & Patel, B. A. (2016). Subchondral properties of the hominoid distal tibia: An
688 indicator of loading during habitually dorsiflexed ankle postures. *American Journal of Physcial*
689 *Anthropology*, 159, 109.

690 Carlson, K. J., Jashashvili, T., Houghton, K., Westaway, M. C., & Patel, B. A. (2013). Joint loads in
691 marsupial ankles reflect habitual bipedalism versus quadrupedalism. *PLoS ONE*, 8, e58811.

692 Carlson, K. J., & Judex, S. (2007). Increased non-linear locomotion alters diaphyseal bone shape. *Journal*
693 *of Experimental Biology*, 210, 3117-3125.

694 Carlson, K. J., Lublinsky, S., & Judex, S. (2008). Do different locomotor modes during growth modulate
695 trabecular architecture in the murine hind limb? *Integrative and Comparative Biology*, 48, 385-393.

696 Chirchir, H., Kivell, T. L., Ruff, C. B., Hublin, J.-J., Carlson, K. J., Zipfel, B., & Richmond, B. G. (2015).
697 Recent origin of low trabecular bone density in modern humans. *Proceedings of the National Academy of*
698 *Sciences*, 112, 366-371.

699 Chirchir, H., Ruff, C. B., Junno, J.-A., & Potts, R. (2017). Low trabecular bone density in recent
700 sedentary modern humans. *American Journal of Physical Anthropology*, 162, 550-560.

701 Clarke, R. J., & Tobias, P. V. (1995). Sterkfontein Member 2 foot bones of the oldest South African
702 hominid. *Science*, 269, 521-524.

703 Cresswell, E. N., Goff, M. G., Nguyen, T. M., Lee, W. X., & Hernandez, C. J. (2015). Spatial
704 relationships between bone formation and mechanical stress within cancellous bone. *Journal of*
705 *Biomechanics*, 49, 222-228.

706 Crompton, R. H. (2015). The hominins: A very conservative tribe? Last common ancestors, plasticity and
707 ecomorphology in Hominidae. Or, what's in a name? *Journal of Anatomy*, 228, 686-699.

708 D'Août, K., Vereecke, E., Schoonaert, K., De Clercq, D., Van Elsacker, L., & Aerts, P. (2004).
709 Locomotion in bonobos (*Pan paniscus*): Differences and similarities between bipedal and quadrupedal
710 terrestrial walking, and a comparison with other locomotor modes. *Journal of Anatomy*, 204, 353-361.

711 Day, M. H., & Wood, B. A. (1968). Functional affinities of the Olduvai Hominid 8 talus. *Man*, 3, 440-
712 455.

713 DeSilva, J. M. (2009). Functional morphology of the ankle and the likelihood of climbing in early
714 hominins. *Proceedings of the National Academy of Sciences*, 106, 6567-6572.

715 DeSilva, J. M. (2010). Revisiting the "midtarsal break". *American Journal of Physical Anthropology*, 141,
716 245-258.

717 DeSilva, J. M., Bonne-Annee, R., Swanson, Z., Gill, C. M., Sobel, M., Uy, J., & Gill, S. V. (2015).
718 Midtarsal break variation in modern humans: Functional causes, skeletal correlates, and paleontological
719 implications. *American Journal of Physical Anthropology*, 156, 543-552.

720 DeSilva, J. M., & Devlin, M. J. (2012). A comparative study of the trabecular bony architecture of the
721 talus in humans, non-human primates, and *Australopithecus*. *Journal of Human Evolution*, 63, 536-551.

722 DeSilva, J. M., Holt, K. G., Churchill, S. E., Carlson, K. J., Walker, C. S., Zipfel, B., & Berger, L. R.
723 (2013). The lower limb and mechanics of walking in *Australopithecus sediba*. *Science*, 340, 1232999.

724 DeSilva, J. M., & Throckmorton, Z. J. (2010). Lucy's flat feet: The relationship between the ankle and
725 rearfoot arching in early hominins. *PLoS One*, 5, e14432.

726 Doran, D. M. (1992). The ontogeny of chimpanzee and pygmy chimpanzee locomotor behavior: A case
727 study of paedomorphism and its behavioral correlates. *Journal of Human Evolution*, 23, 139-157.

Doube, M., Kłosowski, M. M., Arganda-Carreras, I., Cordelières, F. P., Dougherty, R. P., Jackson, J. S., . . . Shefelbine, S. J. (2010). BoneJ: Free and extensible bone image analysis in ImageJ. *Bone*, 47, 1076-1079.

Doube, M., Klosowski, M. M., Wiktorowicz-Conroy, A. M., Hutchinson, J. R., & Shefelbine, S. J. (2011).Trabecular bone scales allometrically in mammals and birds. *Proceedings of the Royal Society B: Biological Sciences*, 278, 3067-3073.

Dunn, R. H., Tocheri, M. W., Orr, C. M., & Jungers, W. L. (2014). Ecological divergence and talar morphology in gorillas. *American Journal of Physical Anthropology*, 153, 526-541.

Ebraheim, N. A., Sabry, F. F., & Nadim, Y. (1999). Internal architecture of the talus: Implication for talar fracture. *Foot & Ankle International*, 20, 794-796.

Ehrlich, P. J., & Lanyon, L. E. (2002). Mechanical strain and bone cell function: A review. *Osteoporosis International*, 13, 688-700.

Elftman, H. (1960). The transverse tarsal joint and its control. *Clinical Orthopaedics*, 16, 41-46.

Elftman, H., & Manter, J. (1935). Chimpanzee and human feet in bipedal walking. *American Journal of Physical Anthropology*, 20, 69-79.

Friston, K. J., Holmes, A. P., Worsley, K. J., Poline, J.-P., Frith, C. D., & Frackowiak, R. S. J. (1995). Statistical parametric maps in functional imaging: A general linear approach. *Human Brain Mapping*, 2, 189–210.

Frost, H. M. (1987). Bone "mass" and the "mechanostat": A proposal. *The Anatomical Record*, 219, 1-9.

Gee, A. H., & Treece, G. M. (2014). Systematic misregistration and the statistical analysis of surface data. *Medical Image Analysis*, 18, 385-393.

Gee, A. H., Treece, G. M., Tonkin, C. J., Black D. M., & Poole, K. E. S. (2015). Association between femur size and a focal defect of the superior femoral neck. *Bone*, 81, 60-66.

Gosman, J. H., & Ketcham, R. A. (2009). Patterns in ontogeny of human trabecular bone from SunWatch Village in the Prehistoric Ohio Valley: General features of microarchitectural change. *American Journal of Physical Anthropology*, 138, 318-332.

Green, R. E., Krause, J., Briggs, A. W., Maricic, T., Stenzel, U., Kircher, M., … Pääbo, S. (2010). A draft sequence of the Neandertal genome. *Science*, 328, 710-722.

Griffin, N. L., D'Août, K., Ryan, T. M., Richmond, B. G., Ketcham, R. A., & Postnov, A. (2010). Comparative forefoot trabecular bone architecture in extant hominids. *Journal of Human Evolution*, 59, 202-213.

Griffin, N. L., Miller, C. E., Schmitt, D., & D'Août, K. (2015). Understanding the evolution of the windlass mechanism of the human foot from comparative anatomy: Insights, obstacles, and future directions. *American Journal of Physical Anthropology*, 156, 1-10.

Gross, T., Kivell, T. L., Skinner, M. M., Nguyen, N. H., & Pahr, D. H. (2014). A CT-image-based framework for the holistic analysis of cortical and trabecular bone morphology. *Palaeontologia Electronica*, 17, 33A.

765 Haile-Selassie, Y., Saylor, B. Z., Deino, A., Levin, N. E., Alene, M., & Latimer, B. M. (2012). A new
766 hominin foot from Ethiopia shows multiple Pliocene bipedal adaptations. *Nature*, 483, 565-570.

767 Harcourt-Smith, W. E. H., & Aiello, L. C. (2004). Fossils, feet and the evolution of human bipedal
768 locomotion. *Journal of Anatomy*, 204, 403-416.

769 Harcourt-Smith, W. E. H., Throckmorton, Z., Congdon, K. A., Zipfel, B., Deane, A. S., Drapeau, M. S.
770 M., . . . DeSilva, J. M. (2015). The foot of *Homo naledi*. *Nature Communications*, 6, 8432.

771 Hatala, K. G., Dingwall, H. L., Wunderlich, R. E., & Richmond, B. G. (2013). Variation in foot strike
772 patterns during running among habitually barefoot populations. *PLoS One*, *8*(1), e52548.

773 Havill, L. M., Allen, M. R., Bredbenner, T. L., Burr, D. B., Nicolella, D. P., Turner, C. H., . . . Mahaney,
774 M. C. (2010). Heritability of lumbar trabecular bone mechanical properties in baboons. *Bone*, 46, 835-
775 840.

776 Hérbert, D., Lebrun, R., & Marivaux, L. (2012). Comparative three-dimensional structure of the
777 trabecular bone in the talus of primates and its relationship to ankle joint loads generated during
778 locomotion. *The Anatomical Record*, 295, 2069-2088.

779 Holowka, N. B., O'Neill, M. C., Thompson, N. E., & Demes, B. (2017). Chimpanzee and human midfoot
780 motion during bipedal walking and the evolution of the longitudinal arch of the foot. *Journal of Human*
781 *Evolution*, 104, 23-31.

782 Hvid, I., Rasmussen, O., Jensen, N. C., & Nielsen, S. (1985). Trabecular bone strength profiles at the
783 ankle joint. *Clinical Orthopaedics and Related Research*, 199, 306-312.

784 Ker, R. F., Bennett, M. B., Bibby, S. R., Kester, R. C., & Alexander, R. M. (1987). The spring in the arch
785 of the human foot. *Nature*, 325, 147-149.

786 Ketcham, R. A., & Ryan, T. M. (2004). Quantification and visualization of anisotropy in trabecular bone.
787 *Journal of Microscopy*, 213, 158-171.

788 Kivell, T. L. (2016). A review of trabecular bone functional adaptation: What have we learned from
789 trabecular analyses in extant hominoids and what can we apply to fossils? *Journal of Anatomy*, 228, 569-
790 594.

791 Kivell, T. L., Skinner, M. M., Lazenby, R., & Hublin, J.-J. (2011). Methodological considerations for
792 analyzing trabecular architecture: An example from the primate hand. *Journal of Anatomy*, 218, 209-225.

793 Kraft, T. S., Venkataraman, V. V., & Dominy, N. J. (2014). A natural history of human tree climbing.
794 *Journal of Human Evolution*, 71, 105-118.

795 Kuo, S., DeSilva, J. M., Devlin, M. J., McDonald, G., & Morgan, E. F. (2013). The effect of the Achilles
796 tendon on trabecular structure in the primate calcaneus. *The Anatomical Record*, 296, 1509-1517.

797 Lanyon, L. E. (1974). Experimental support for the trajectorial theory of bone structure. *The Journal of*
798 *Bone and Joint Surgery*, 56, 160-166.

799 Latimer, B., Ohman, J. C., & Lovejoy, C. O. (1987). Talocrural joint in African hominoids: Implications
800 for *Australopithecus afarensis*. *American Journal of Physical Anthropology*, 74, 155-175.

Lazenby, R. A., Skinner, M. M., Kivell, T. L., & Hublin, J.-J. (2011). Scaling VOI size in 3D μCT studies of trabecular bone: A test of the over-sampling hypothesis. *American Journal of Physical Anthropology*, 144, 196-203.

Lewis, O. J. (1980a). The joints of the evolving foot. Part I. The ankle joint. *Journal of Anatomy*, 130, 527-543.

Lewis, O. J. (1980b). The joints of the evolving foot. Part II. The intrinsic joints. *Journal of Anatomy*, 130, 833-857.

Lewis, O. J. (1980c). The joints of the evolving foot. Part III. The fossil evidence. *Journal of Anatomy*, 131, 275-298.

Lieberman, D. E. (1996). How and why humans grow thin skulls: Experimental evidence for systemic cortical robusticity. *American Journal of Physical Anthropology*, 101, 217-236.

Lieberman, D. E., Venkadesan, M., Werbel, W. A., Daoud, A. I., D'Andrea, S., Davis, I. S., . . . Pitsiladis, Y. (2010). Foot strike patterns and collision forces in habitually barefoot versus shod runners. *Nature*, 463(7280), 531-535.

Lisowski, F. P., Albrecht, G. H., & Oxnard, C. E. (1974). The form of the talus in some higher primates: A multivariate study. *American Journal of Physical Anthropology*, 41, 191-216.

Lisowski, F. P., Albrecht, G. H., & Oxnard, C. E. (1976). African fossil tali: Further multivariate morphometric studies. *American Journal of Physical Anthropology*, 45, 5-18.

Lovejoy, C. O., McCollum, M. A., Reno, P. L., & Rosenman, B. A. (2003). Developmental biology and human evolution. *Annual Review of Anthropology*, 32, 85-109.

MacLatchy, L., & Müller, R. (2002). A comparison of the femoral head and neck trabecular architecture of *Galago* and *Perodicticus* using micro-computed tomography (μCT). *Journal of Human Evolution*, 43, 89-105.

Maga, M., Kappelman, J., Ryan, T. M., & Ketcham, R. A. (2006). Preliminary observations on the calcaneal trabecular microarchitecture of extant large-bodied hominoids. *American Journal of Physical Anthropology*, 129, 410-417.

Maquer, G., Musy, S. N., Wandel, J., Gross, T., & Zysset, P. K. (2015). Bone volume fraction and fabric anisotropy are better determinants of trabecular bone stiffness than other morphological variables. *Journal of Bone and Mineral Research*, 30, 1000-1008.

Mazurier, A., Nakatsukasa, M., & Macchiarelli, R. (2010). The inner structural variation of the primate tibial plateau characterized by high-resolution microtomography. Implications for the reconstruction of fossil locomotor behaviours. *Comptes Rendus Palevol*, 9, 349-359.

Morgan, E. F., & Keaveny, T. M. (2001). Dependence of yield strain of human trabecular bone on anatomic site. *Journal of Biomechanics*, 34, 569-577.

Morris, J. M. (1977). Biomechanics of the foot and ankle. *Clinical Orthopaedics and Related Research*, 122, 10-17.

Nowakowski, A. M., Deyhle, H., Zander, S., Leumann, A., & Müller-Gerbl, M. (2013). Micro CT analysis of the subarticular bone structure in the area of the talar trochlea. *Surgical and Radiologic Anatomy*, 35, 283-293.

Odgaard, A. (1997). Three-dimensional methods for quantification of cancellous bone architecture. *Bone*, 20, 315-328.

O'Neill, M. C., Lee, L.-F., Demes, B., Thompson, N. E., Larson, S. G., Stern Jr, J. T., & Umberger, B. R. (2015). Three-dimensional kinematics of the pelvis and hind limbs in chimpanzee (*Pan troglodytes*) and human bipedal walking. *Journal of Human Evolution*, 86, 32-42.

Oxnard, C. E., & Lisowski, F. P. (1980). Functional articulation of some hominoid foot bones:

Implications for the Olduvai (Hominid 8) foot. *American Journal of Physical Anthropology*, 52, 107-117.

Pal, G. P., & Routal, R. V. (1998). Architecture of the cancellous bone of the human talus. *The Anatomical Record*, 252, 185-193.

Patel, B. A., & Carlson, K. J. (2007). Bone density spatial patterns in the distal radius reflect habitual hand postures adopted by quadrupedal primates. *Journal of Human Evolution*, 52, 130-141.

Paternoster, L., Lorentzon, M., Lehtimäki, T., Eriksson, J., Kähönen, M., Raitakari, O., . . . Ohlsson, C. (2013). Genetic determinants of trabecular and cortical volumetric bone mineral densities and bone microstructure. *PLoS Genetics*, 9, e1003247.

Pearson, O. M., & Lieberman, D. E. (2004). The aging of Wolff's 'law': Ontogeny and responses to mechanical loading in cortical bone. *Yearbook of Physical Anthropology*, 47, 63-99.

Pettersson, U., Nilsson, M., Sundh, V., Mellström, D., & Lorentzon, M. (2010). Physical activity is the strongest predictor of calcaneal peak bone mass in young Swedish men. *Osteoporosis International*, 21, 447-455.

Polk, J. D., Blumenfeld, J., & Ahluwalia, D. (2008). Knee posture predicted from subchondral apparent density in the distal femur: An experimental validation. *The Anatomical Record*, 291, 293-302.

Polk, J. D., Williams, S. A., Peterson, J. V., Roseman, C. C., & Godfrey, L. R. (2010). Subchondral bone apparent density and locomotor behavior in extant primates and subfossil lemurs Hadropithecus and Pachylemur. International Journal of Primatology, 31, 275-299.

Pontzer, H., Lieberman, D. E., Momin, E., Devlin, M. J., Polk, J. D., Hallgrímsson, B., & Cooper, D. M. L. (2006). Trabecular bone in the bird knee responds with high sensitivity to changes in load orientation. *The Journal of Experimental Biology*, 209, 57-65.

Pontzer, H., Raichlen, D. A., & Rodman, P. S. (2014). Bipedal and quadrupedal locomotion in chimpanzees. *Journal of Human Evolution*, 66, 64-82.

Pontzer, H., Raichlen, D. A., & Sockol, M. D. (2009). The metabolic cost of walking in humans, chimpanzees, and early hominins. *Journal of Human Evolution*, 56, 43-54.

Prang, T. C. (2015). Rearfoot posture of *Australopithecus sediba* and the evolution of the hominin longitudinal arch. *Scientific Reports*, 5, 17677.

Prang, T. C. (2016). The subtalar joint complex of *Australopithecus sediba*. *Journal of Human Evolution*, 90, 105-119.

Raichlen, D. A., Gordon, A. D., Foster, A. D., Webber, J. T., Sukhdeo, S. M., Scott, R. S., . . . Ryan, T. M. (2015). An ontogenetic framework linking locomotion and trabecular bone architecture with applications for reconstructing hominin life history. *Journal of Human Evolution*, 81, 1-12.

878 R Core Team. (2016). R: A language and environment for statistical computing. R Foundation for
879 Statistical Computing, Vienna, Austria. URL https://www.R-project.org/

880 Robling, A. G., Hinant, F. M., Burr, D. B., & Turner, C. H. (2002). Improved bone structure and strength
881 after long-term mechanical loading is greatest if loading is separated into short bouts. *Journal of Bone*
882 *and Mineral Research*, 17, 1545-1554.

883 Rubin, C. T., & Lanyon, L. E. (1985). Regulation of bone mass by mechanical strain magnitude. *Calcified*
884 *Tissue International*, 37, 411-417.

885 Ruff, C. B. (2005). Mechanical determinants of bone form: Insights from skeletal remains. *Journal of*
886 *Musculoskeletal Neuronal Interactions*, 5, 202-212.

887 Ruff, C., Holt, B., & Trinkaus, E. (2006). Who's afraid of the big bad Wolff? "Wolff's law" and bone
888 functional adaptation. *American Journal of Physical Anthropology*, 129, 484-498.

889 Ruff, C. B., & Runestad, J. A. (1992). Primate limb bone structural adaptations. *Annual Review of*
890 *Anthropology*, 21, 407-433.

891 Ruff, C. B., Trinkaus, E., Walker, A., & Larsen, C. S. (1993). Postcranial robusticity in *Homo*, I:
892 Temporal trends and mechanical interpretation. *American Journal of Physical Anthropology*, 91, 21-53.

893 Ryan, T. M., & Ketcham, R. A. (2002a). The three-dimensional structure of trabecular bone in the
894 femoral head of strepsirrhine primates. *Journal of Human Evolution*, 43, 1-26.

895 Ryan, T. M., & Ketcham, R. A. (2002b). Femoral head trabecular bone structure in two omomyid
896 primates. *Journal of Human Evolution*, 43, 241-263.

897 Ryan, T. M., & Krovitz, G. E. (2006). Trabecular bone ontogeny in the human proximal femur. *Journal*
898 *of Human Evolution*, 51, 591-602.

899 Ryan, T. M., & Shaw, C. N. (2015). Gracility of the modern *Homo sapiens* skeleton is the result of
900 decreased biomechanical loading. *Proceedings of the National Academy of Sciences*, 112, 372-377.

901 Ryan, T. M., van Rietbergen, B., & Krovitz, G. (2007). Mechanical adaptation of the trabecular bone in
902 the growing human femur and humerus. *American Journal of Physical Anthropology*, 44, 203.

903 Sarringhaus, L. A., MacLatchy, L. M., & Mitani, J. C. (2014). Locomotor and postural development of
904 wild chimpanzees. *Journal of Human Evolution*, 66, 29-38.

905 Scherf, H., & Tilgner, R. (2009). A new high-resolution computed tomography (CT) segmentation
906 method for trabecular bone architectural analysis. *American Journal of Physical Anthropology*, 140, 39-
907 51.

908 Scherf, H., Wahl, J., Hublin, J.-J., & Harvati, K. (2015). Patterns of activity adaptation in humeral
909 trabecular bone in Neolithic humans and present-day people. *American Journal of Physical Anthropology*,
910 159, 106-115.

911 Schiff, A., Li, J., Inoue, N., Masuda, K., Lidtke, R., & Muehleman, C. (2007). Trabecular angle of the
912 human talus is associated with the level of cartilage degeneration. *Journal of Musculoskeletal and*
913 *Neuronal Interactions*, 7, 224-230.

914 Schneider, C. A., Rasband, W. S., & Eliceiri, K. W. (2012). NIH Image to ImageJ: 25 years of image
915 analysis. *Nature Methods*, 9, 671-675.

916 Schoonaert, K., D'Août, K., Samuel, D., Talloen, W., Nauwelaerts, S., Kivell, T. L., & Aerts, P. (2016).
917 Gait characteristics and spatio-temporal variables of climbing in bonobos (*Pan paniscus*). *American*
918 *Journal of Primatology*, 78, 1165-1177.

919 Schulte, F. A., Ruffoni, D., Lambers, F. M., Christen, D., Webster, D. J., Kuhn, G., & Müller, R. (2013).
920 Local mechanical stimuli regulate bone formation and resorption in mice at the tissue level. *PLoS ONE*, 8,
921 e62172.

922 Scott, S. H., & Winter, D. A. (1991). Talocrural and talocalcaneal joint kinematics and kinetics during the
923 stance phase of walking. *Journal of Biomechanics*, 24, 743-752.

924 Siegler, S., Chen, J., & Schneck, C. D. (1988). The three-dimensional kinematics and flexibility
925 characteristics of the human ankle and subtalar joints: Part I: Kinematics. *Journal of Biomechanical*
926 *Engineering*, 110, 364-373.

927 Singh, I. (1978). The architecture of cancellous bone. *Journal of Anatomy*, 127, 305-310.

928 Sinha, D. N. (1985). Cancellous structure of tarsal bones. *Journal of Anatomy*, 140, 111-117.

929 Smith, R. J., & Jungers, W. L. (1997). Body mass in comparative primatology. *Journal of Human*
930 *Evolution*, 32, 523-559.

931 Skerry, T. M., & Lanyon, L. E. (1995). Interruption of disuse by short duration walking exercise does not
932 prevent bone loss in the sheep calcaneus. *Bone*, 16, 269-274.

933 Skinner, M. M., Stephens, N. B., Tsegai, Z. J., Foote, A. C., Nguyen, N. H., Gross, T., Pahr, D. H.,
934 Hublin, J.-J., & Kivell, T. L. (2015). Human-like hand use in *Australopithecus africanus*. *Science*, 347,
935 395-399.

936 Sode, M., Burghardt, A. J., Nissenson, R. A., & Majumdar, S. (2008). Resolution dependence of the non-
937 metric trabecular structure indices. *Bone*, 42, 728-736.

938 Sockol, M. D., Raichlen, D. A., & Pontzer, H. (2007). Chimpanzee locomotor energetics and the origin of
939 human bipedalism. *Proceedings of the National Academy of Sciences*, 104(30), 12265-12269.

940 Stauber, M., Rapillard, L., van Lenthe, G. H., Zysset, P., & Müller, R. (2006). Importance of individual
941 rods and plates in the assessment of bone quality and their contribution to bone stiffness. *Journal of Bone*
942 *and Mineral Research*, 21, 586-595.

943 Stern, J. T., & Susman, R. L. (1983). The locomotor anatomy of *Australopithecus afarensis*. *American*
944 *Journal of Physical Anthropology*, 60, 279-317.

945 Su, A. (2011). *The Functional Morphology of Subchondral and Trabecular Bone in the Hominoid*
946 *Tibiotalar Joint*. (Doctoral dissertation, Stony Brook University). Retrieved from
947 https://dspace.sunyconnect.suny.edu/handle/1951/56131

948 Su, A., & Carlson, K. J. (2017). Comparative analysis of trabecular bone structure and orientation in
949 South African hominin tali. *Journal of Human Evolution*, 106, 1-18.

950 Su, A., Wallace, I. J., & Nakatsukasa, M. (2013). Trabecular bone anisotropy and orientation in an Early
951 Pleistocene hominin talus from East Turkana, Kenya. *Journal of Human Evolution*, 64, 667-677.

952 Susman, R. L. (1983). Evolution of the human foot: Evidence from Plio-Pleistocene hominids. *Foot &*
953 *Ankle*, 3, 365-376.

954 Sutherland, D. H., Olshen, R., Cooper, L., & Woo, S. L. Y. (1980). The development of mature gait.
955 *Journal of Bone and Joint Sur*gery, 62A, 336-353.

956 Takechi, H., Ito, S., Takada, T., & Nakayama, H. (1982). Trabecular architecture of the ankle joint.
957 *Anatomia Clinica*, 4, 227-233.

958 Thompson, N. E., Holowka, N. B., O'Neill, M. C., & Larson, S. G. (2014). Brief communication:
959 Cineradiographic analysis of the chimpanzee (*Pan troglodytes*) talonavicular and calcaneocuboid joints.
960 *American Journal of Physical Anthropology*, 154, 604-608.

961 Thorpe, S. K. S., Crompton, R. H., & Wang, W. J. (2004). Stresses exerted in the hindlimb muscles of
962 common chimpanzees (*Pan troglodytes*) during bipedal locomotion. *Folia Primatologica*, 75, 253-265.

963 Treece, G. M., Gee, A. H., Mayhew, P. M., & Poole, K. E. S. (2010). High resolution cortical bone
964 thickness measurement from clinical CT data. *Medical Image Analysis*, 14, 276-290.

965 Treece, G. M., Poole, K. E. S., & Gee, A. H. (2012). Imaging the femoral cortex: Thickness, density and
966 mass from clinical CT. *Medical Image Analysis*, 16, 952-965.

967 Tsegai, Z. J., Kivell, T. L., Gross, T., Nguyen, N. H., Pahr, D. H., Smaers, J. B., & Skinner, M. M.
968 (2013). Trabecular bone structure correlates with hand posture and use in hominoids. *PLoS One*, 8,
969 e78781.

970 Tsegai, Z. J., Skinner, M. M., Pahr, D. H., Hublin, J.-J., & Kivell, T. L. (2016a). Systemic patterns of
971 trabecular structure in *Homo* and *Pan*: Evaluating inter- and intraspecific variability across anatomical
972 sites. *American Journal of Physical Anthropology*, 159, 318.

973 Tsegai, Z. J., Stephens, N. S., Treece, G., Skinner, M. M., Kivell, K. L., & Gee, A. (2016b). Cortical bone
974 mapping: An application to hand and foot bones in hominoids. *Comptes Rendus Palevol*,
975 http://doi.org/10.1016/j.crpv.2016.11.001

976 Turner, A. S. (2001). Animal models of osteoporosis – necessity and limitations. *European Cells and*
977 *Materials*, 1, 66-81.

978 Venkataraman, V. V., Kraft, T. S., DeSilva, J. M., & Dominy, N. J. (2013a). Phenotypic plasticity of
979 climbing-related traits in the ankle joint of great apes and rainforest hunter-gatherers. *Human Biology*, 85,
980 309-328.

981 Venkataraman, V. V., Kraft, T. S., & Dominy, N. J. (2013b). Tree climbing and human evolution.
982 *Proceedings of the National Academy of Sciences*, 110, 1237-1242.

983 Vereecke, E., D'Août, K., De Clercq, D., Van Elsaker, L., & Aerts, P. (2003). Dynamic plantar pressure
984 distribution during terrestrial locomotion of bonobos (*Pan paniscus*). *American Journal of Physical*
985 *Anthropology*, 120, 373-383.

986 Wallace, I. J., Kwaczala, A. T., Judex, S., Demes, B., & Carlson, K. J. (2013). Physical activity
987 engendering loads from diverse directions augments the growing skeleton. *Journal of Musculoskeletal*
988 *and Neuronal Interactions*, 13, 283-288.

989 Wallace, I. J., Middleton, K. M., Lublinsky, S., Kelly, S. A., Judex, S., Garland, T., & Demes, B. (2010).
990 Functional significance of genetic variation underlying limb bone diaphyseal structure. *American Journal*
991 *of Physical Anthropology*, 143, 21-30.

992 Wan, L., de Asla, R. J., Rubash, H. E., & Li, G. (2006). Determination of *in-vivo* articular cartilage
993 contact areas of human talocrural joint under weightbearing conditions. *Osteoarthritis and Cartilage*, 14,
994 1294-1301.

995 Wang, W., Abboud, R. J., Günther, M. M., & Crompton, R. H. (2014). Analysis of joint force and torque
996 for the human and non-human ape foot during bipedal walking with implications for the evolution of the
997 foot. *Journal of Anatomy*, 225, 152-166.

998 Whitehouse, W. J. (1974). The quantitative morphology of anisotropic trabecular bone. *Journal of*
999 *Microscopy*, 101, 153-168.

1000 Wickham, H. (2009). *ggplot2: Elegant graphics for data analysis*. New York: Springer-Verlag.

1001 Worsley, K. J., Taylor, J. E., Carbonell, F., Chung, M. K., Duerden, E., Bernhardt, B., . . . Evans, A. C.
1002 (2009) SurfStat: A Matlab toolbox for the statistical analysis of univariate and multivariate surface and
1003 volumetric data using linear mixed effects models and random field theory. NeuroImage Organization for
1004 Human Brain Mapping Annual Meeting, 47, S102.

1005 Zeininger, A., Patel, B. A., Zipfel, B., Carlson, K. J. (2016). Trabecular architecture in the StW 352 fossil
1006 hominin calcaneus. *Journal of Human Evolution*, 97, 145-158.

1007 Zeininger, A., Richmond, B. G., & Hartman, G. (2011). Metacarpal head biomechanics: A comparative
1008 backscattered electron image analysis of trabecular bone mineral density in *Pan troglodytes*, *Pongo*
1009 *pygmaeus*, and *Homo sapiens*. *Journal of Human Evolution*, 60, 703-710.

1010 Zipfel, B., DeSilva, J. M., Kidd, R. S., Carlson, K. J., Churchill, S. E., & Berger, L. R. (2011). The foot
1011 and ankle of *Australopithecus sediba*. *Science*, 333, 1417-1420.

Table 1. Study sample

Taxon	Body mass (kg)[3]	Locomotor behaviour	Tibia	Talus	Paired	Scan resolution (µm)	Relative resolution[4]
Homo sapiens[1]	62.1-72.1	Biped	8	9	7	40	5.72-9.06
Pan troglodytes verus[2]	41.6-46.3	Arboreal/knuckle-walker	10	13	8	35	5.46-11.59

[1] Anthropological Collection of Institute of Zoology and Anthropology, University of Göttingen
[2] Max Planck Institute for Evolutionary Anthropology
[3] Sex specific mean body mass (F-M). Body masses from Smith and Jungers (1997)
[4] Relative resolution = mean trabecular thickness (mm)/resolution(mm)

Table 2. Mean and standard deviation of trabecular and cortical parameters in the talus and distal tibia of *Homo* and *Pan*. Results of Mann-Whitney U test between taxa are shown, with significant differences in bold.

Element	Taxon	Tb.Th (mm)	BV.TV (%)	DA	BS/BV(mm^{-1})	Cortical thickness (mm)
Talus	*Homo*	0.26 (0.03)	24.77 (2.17)	0.14 (0.07)	0.32 (0.05)	0.45 (0.06)
	Pan	0.31 (0.04)	34.65 (2.63)	0.02 (0.02)	0.19 (0.02)	0.88 (0.19)
	Significance	**<0.01**	**<0.01**	**<0.01**	**<0.01**	**<0.01**
Tibia	*Homo*	0.25 (0.04)	19.92 (2.87)	0.29 (0.10)	0.45 (0.08)	0.63 (0.07)
	Pan	0.23 (0.02)	24.17 (3.43)	0.32 (0.06)	0.31 (0.06)	1.13 (0.19)
	Significance	0.17	**0.02**	0.51	**<0.01**	**<0.01**

Table 3. Results of Spearman's correlation test to test relationship between trabecular parameters within *Homo* and *Pan* in the talus and distal tibia.

Element	Taxon	Parameter	Tb.Th	BV/TV	BS/BV	DA
Talus	*Homo*	BV/TV	0.42	-		
		BS/BV	-0.18	**-0.92****	-	
		DA	**-0.82****	-0.45	0.28	-
		CTh	0.57	0.50	-0.30	**-0.72***
	Pan	BV/TV	**0.59***	-		
		BS/BV	-0.10	**-0.80****	-	
		DA	**-0.98****	**-0.66****	0.16	-
		CTh	**0.84****	**0.63***	-0.24	**-0.80****
Tibia	*Homo*	BV/TV	0.71	-		
		BS/BV	**-0.83****	**-0.90****	-	
		DA	**-0.74***	-0.50	0.69	-
		CTh	0.31	0.07	-0.07	-0.02
	Pan	BV/TV	**0.75***	-		
		BS/BV	**-0.67***	**-0.95****	-	
		DA	**-0.71***	-0.62	0.41	-
		CTh	**0.82****	**0.65***	**-0.66***	-0.44

P-values indicated as $p < 0.05$ * and $p < 0.01$ **

Table 4. Results of principal component analyses showing percentage variance and loading for each principal component. The analysis was conducted separately for the talus and tibia, including Tb.Th, BV/TV, DA, BS/BV, and cortical thickness.

Element	Parameter	PC1	PC2	PC3	PC4	PC5
Talus	% variance	82.64	10.27	4.35	2.43	0.31
	(cumulative)	(82.64)	(92.90)	(97.26)	(99.69)	(100.00)
	Tb.Th	**0.41**	**0.70**	0.30	**0.50**	-0.08
	BV/TV	**0.48**	-0.28	0.09	0.08	**0.82**
	DA	**-0.44**	-0.21	**0.85**	0.16	0.07
	BS/BV	**-0.43**	**0.62**	-0.05	**-0.40**	**0.51**
	Cortical thickness	**0.46**	0.05	**0.41**	**-0.75**	-0.22
Tibia	% variance	56.45	34.41	5.41	2.88	0.86
	(cumulative)	(56.45)	(90.85)	(96.26)	(99.14)	(100.00)
	Tb.Th	0.27	**-0.65**	0.03	**-0.71**	-0.06
	BV/TV	**0.57**	0.13	**0.42**	0.06	**0.69**
	DA	-0.30	**0.62**	0.29	-0.67	0.02
	BS/BV	**-0.55**	-0.22	-0.36	-0.09	**0.72**
	Cortical thickness	**0.46**	0.37	**-0.78**	-0.20	**0**.05

High loadings (i.e. greater than 0.40) are shown in bold

Table 5. The relationship between bone structure and bone size in *Homo* and *Pan*. Results of OLS regression and Pearson's correlation for each trabecular parameter and cortical thickness against the geometric mean of several measurements, used as a proxy for bone size.

Taxon	Element	Parameter	Pearson's *r*	Slope	Lower 95% CI	Upper 95% CI	*P*-value	R^2
Homo	Talus	Tb.Th	-0.40	-0.51	-1.58	0.57	0.30	0.15
		BV/TV	-0.48	-0.52	-1.37	0.34	0.20	0.23
		DA	0.10	2.01	-4.28	8.29	0.48	0.08
		BS/BV	0.33	0.59	-1.23	2.41	0.47	0.08
		CTh	0.12	0.23	-1.23	1.70	0.72	0.02
	Tibia	Tb.Th	0.27	0.53	-1.47	2.53	0.54	0.07
		BV/TV	0.55	1.11	-0.57	2.80	0.16	0.30
		DA	0.09	-0.05	-6.71	6.61	0.99	0.00
		BS/BV	-0.51	-1.35	-3.56	0.87	0.19	0.27
		CTh	0.25	0.38	-1.19	1.95	0.57	0.06
Pan	Talus	Tb.Th	0.29	0.55	-0.79	1.89	0.39	0.07
		BV/TV	-0.05	-0.06	-0.88	0.76	0.87	0.00
		DA	-0.11	-2.97	-11.57	5.62	0.46	0.05
		BS/BV	0.12	0.25	-1.15	1.65	0.70	0.01
		CTh	0.19	0.60	-1.55	2.75	0.55	0.03
	Tibia	Tb.Th	0.37	0.74	-0.64	2.11	0.25	0.16
		BV/TV	0.05	0.16	-1.70	2.03	0.84	0.01
		DA	-0.35	-1.22	-3.98	1.54	0.34	0.11
		BS/BV	-0.04	-0.04	-3.36	3.27	0.98	0.00
		CTh	0.28	0.80	-1.32	2.93	0.41	0.09

Table 6. Results of Pearson's correlation test to test relationship of each trabecular parameter and cortical thickness between the talus and distal tibia in *Homo* and *Pan*.

Taxa	Parameter	Pearson's *r*	*P*-value
Homo	Tb.Th	0.83	**0.02**
	BV/TV	0.72	0.07
	DA	0.55	0.20
	BS/BV	0.83	**0.02**
	Cortical thickness	0.43	0.33
Pan	Tb.Th	0.86	**0.01**
	BV/TV	0.80	**0.02**
	DA	0.56	0.15
	BS/BV	0.81	**0.02**
	Cortical thickness	0.92	**<0.01**

Significant correlations are shown in bold ($p < 0.05$)

Fig 1. Processing steps for trabecular and cortical bone analysis for a *Pan* distal tibia. a) Segmented microCT scan. b) Segmented trabecular bone. c) Inner mask, where trabecular bone and internal region of the bone are assigned different grey values, and the cortical bone has been removed. A background grid and sampling sphere are applied to calculate trabecular structure throughout the bone. d) Tetrahedral mesh with colour scalars representing trabecular bone volume fraction. e) Unsegmented voxel data. f) Process of measurement of cortical thickness. g) Cortical thickness values mapped to a subject-specific surface. h) Each subject-specific surface (green) is registered to a canonical surface (red) for interspecific comparisons.

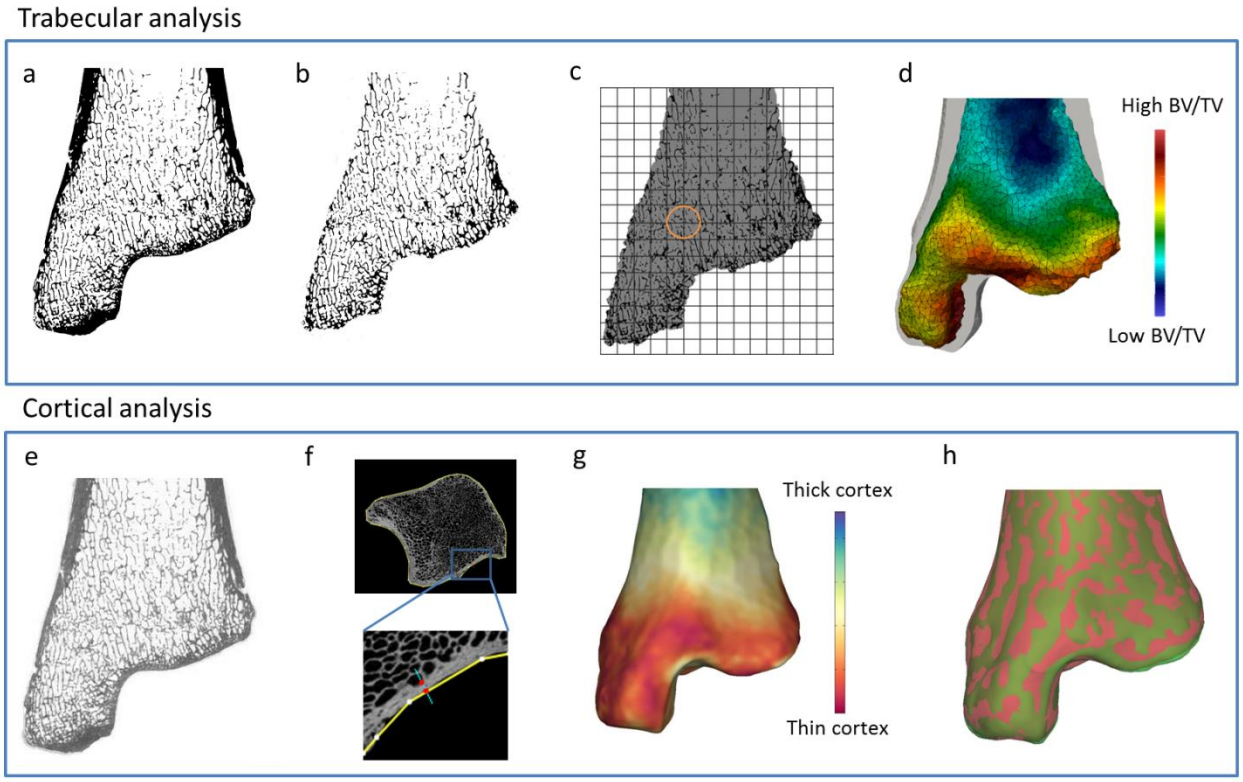

Fig 2. Extracted cubes of trabecular bone from approximately the same location in the talus and distal tibia of *Homo* and *Pan*.

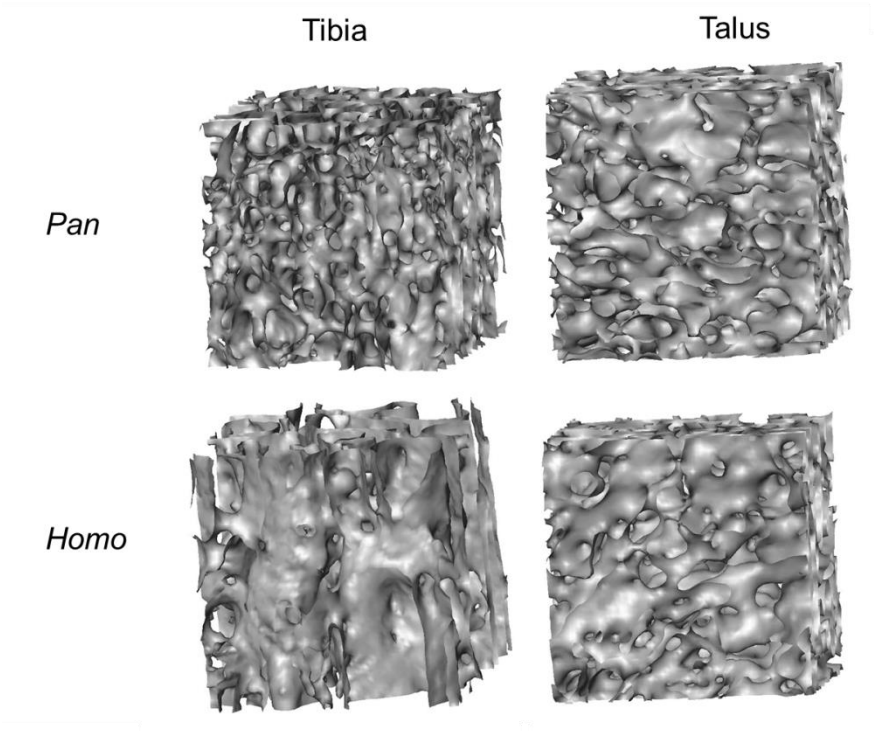

Fig 3. PC1 and PC2 for trabecular and cortical structure of the talus and distal tibia of *Pan* (blue) and *Homo* (red).

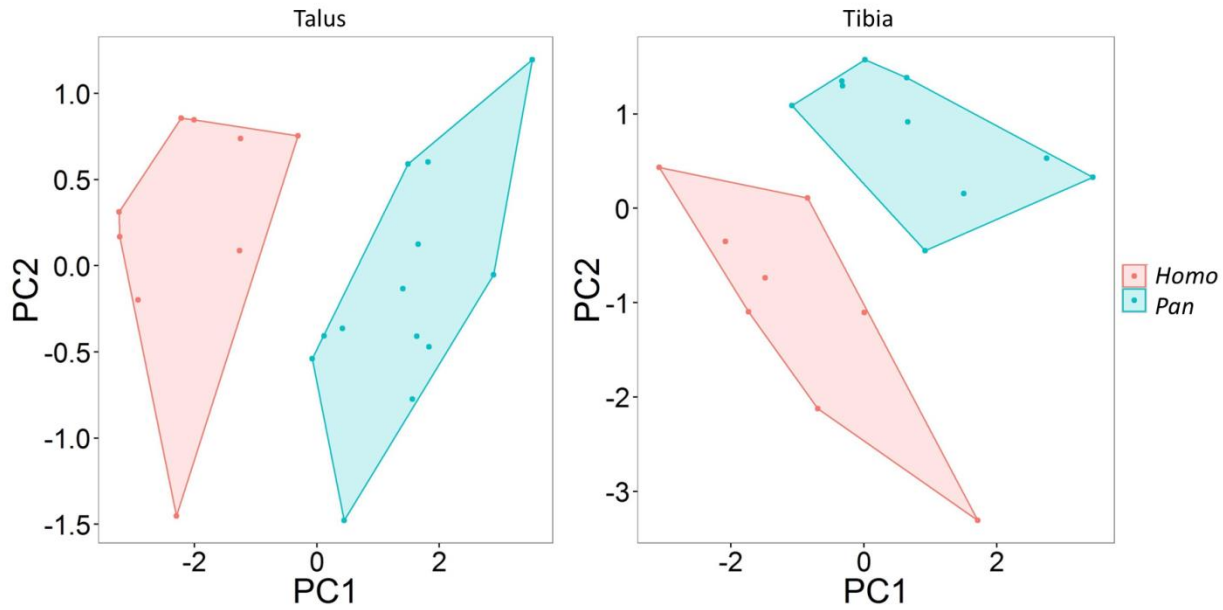

Fig 4. Relationship between talus size and trabecular and cortical parameters in *Pan* (blue) and *Homo* (red). The $\log_{10}$ OLS regression lines are shown independently for *Pan* (blue) and *Homo* (red).

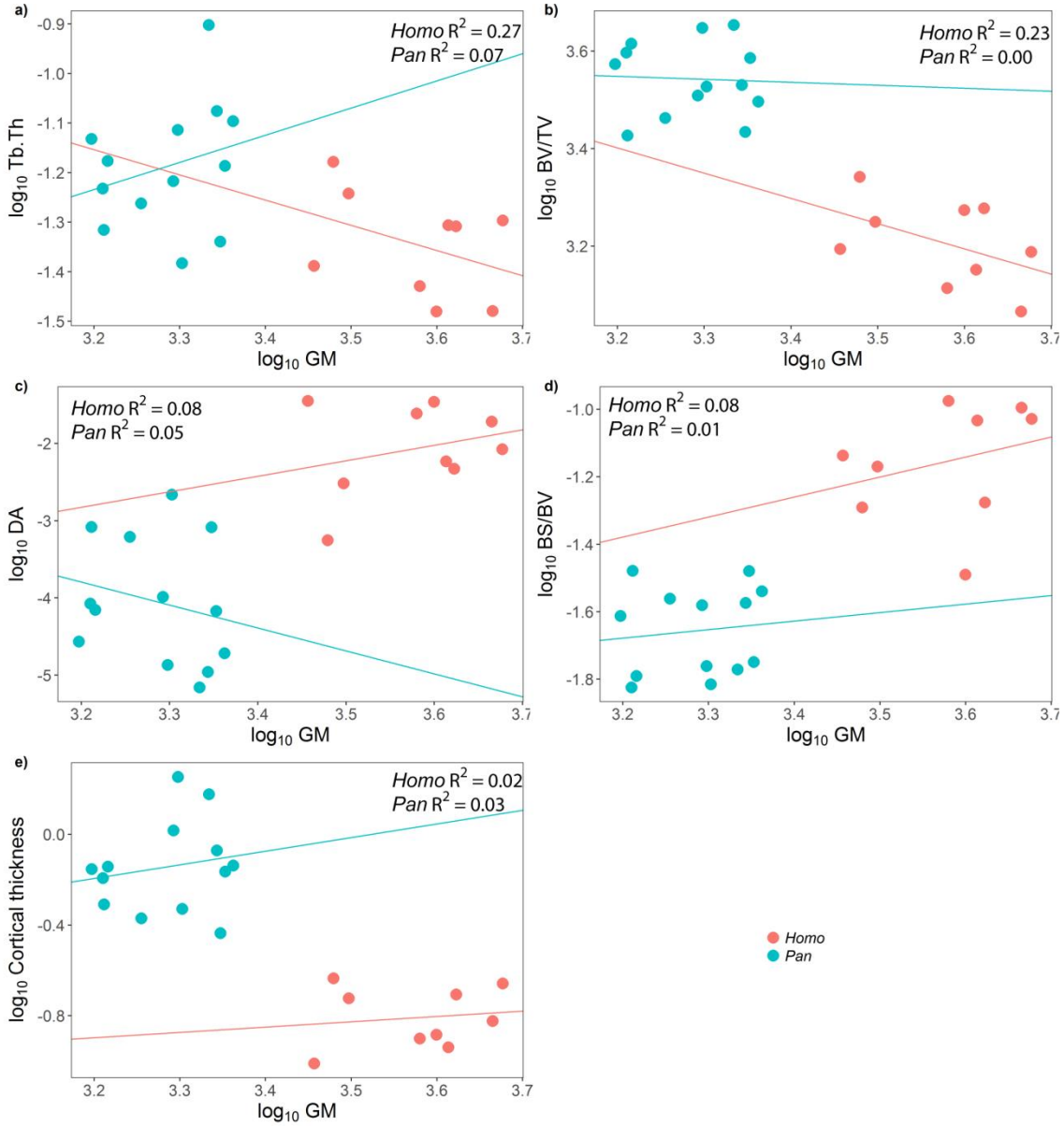

Fig 5. Relationship between tibia size and trabecular and cortical parameters in *Pan* (blue) and *Homo* (red). The $\log_{10}$ OLS regression lines are shown independently for *Pan* (blue) and *Homo* (red).

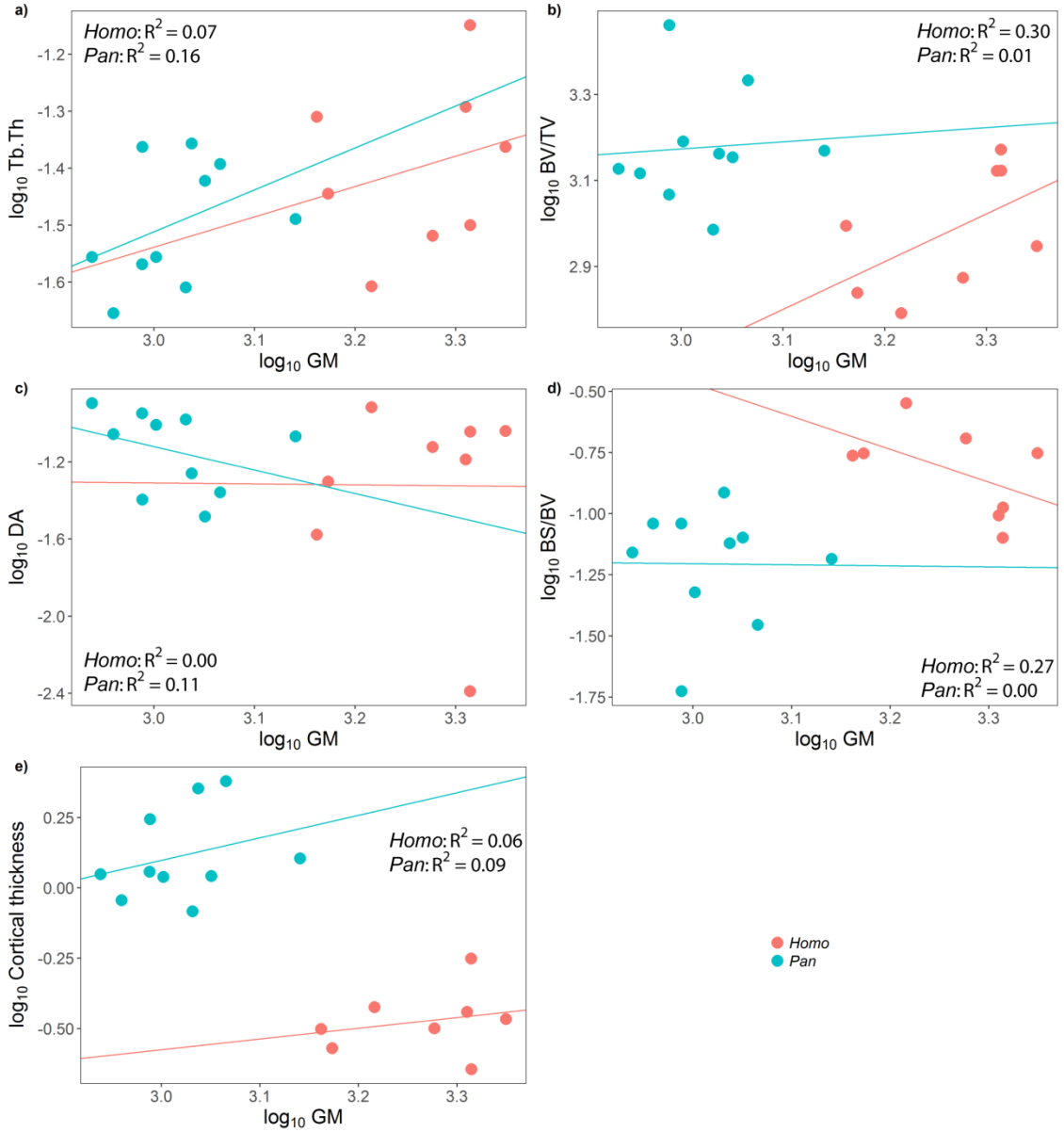

Fig 6. Comparison of trabecular and cortical structure between the talus and tibia in *Pan* (blue) and *Homo* (red). The $\log_{10}$ RMA regression lines are shown independently for *Pan* (blue) and *Homo* (red).

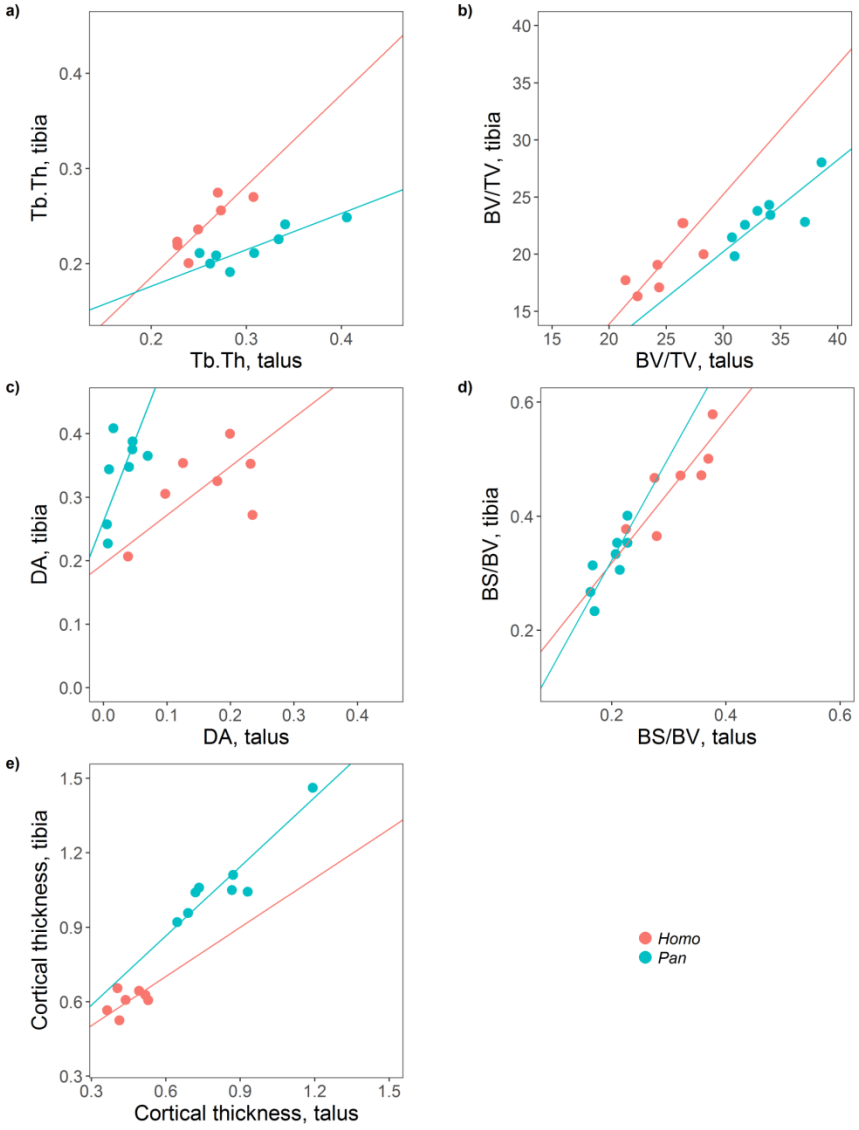

Fig 7. Morphometric maps of BV/TV in the talus in one individual of *Homo* (a-e) and *Pan* (f-j) in (from top to bottom) dorsal view, mid-transverse plane, anterior view, coronal plane (in the centre of the trochlea), and sagittal plane (in the centre of the trochlea). Each specimen is scaled to its own data range, as shown in the scale bars. Black arrows indicate regions described in the text.

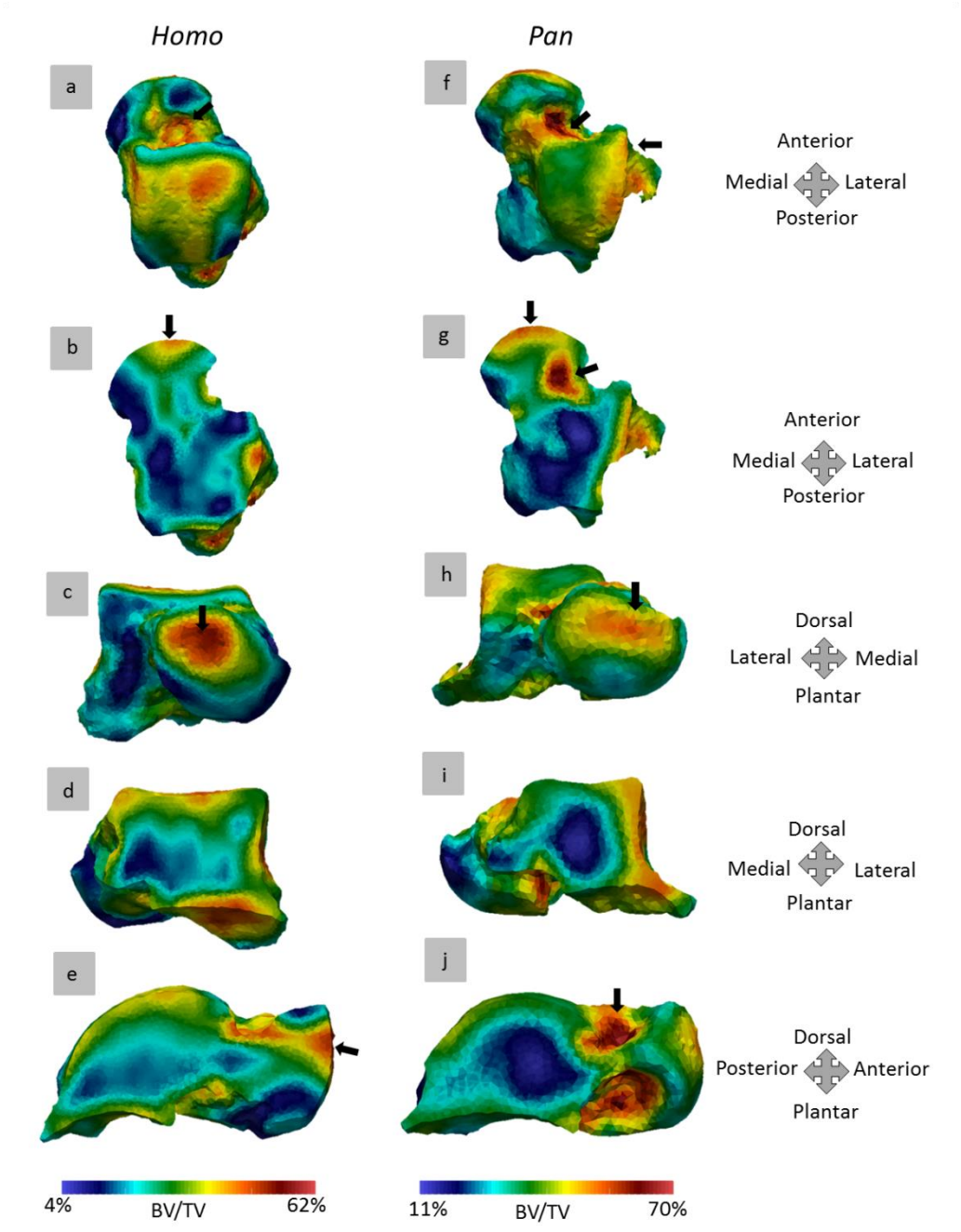

Fig 8. Morphometric maps of BV/TV in the tibia in one individual of *Homo* (a-e) and *Pan* (f-j) in (from top to bottom) distal view, mid-sagittal plane of distal tibia, anterior view and mid-coronal plane of distal tibia. Each specimen is scaled to its own data range, as shown in the scale bars. Black arrows indicate regions described in the text.

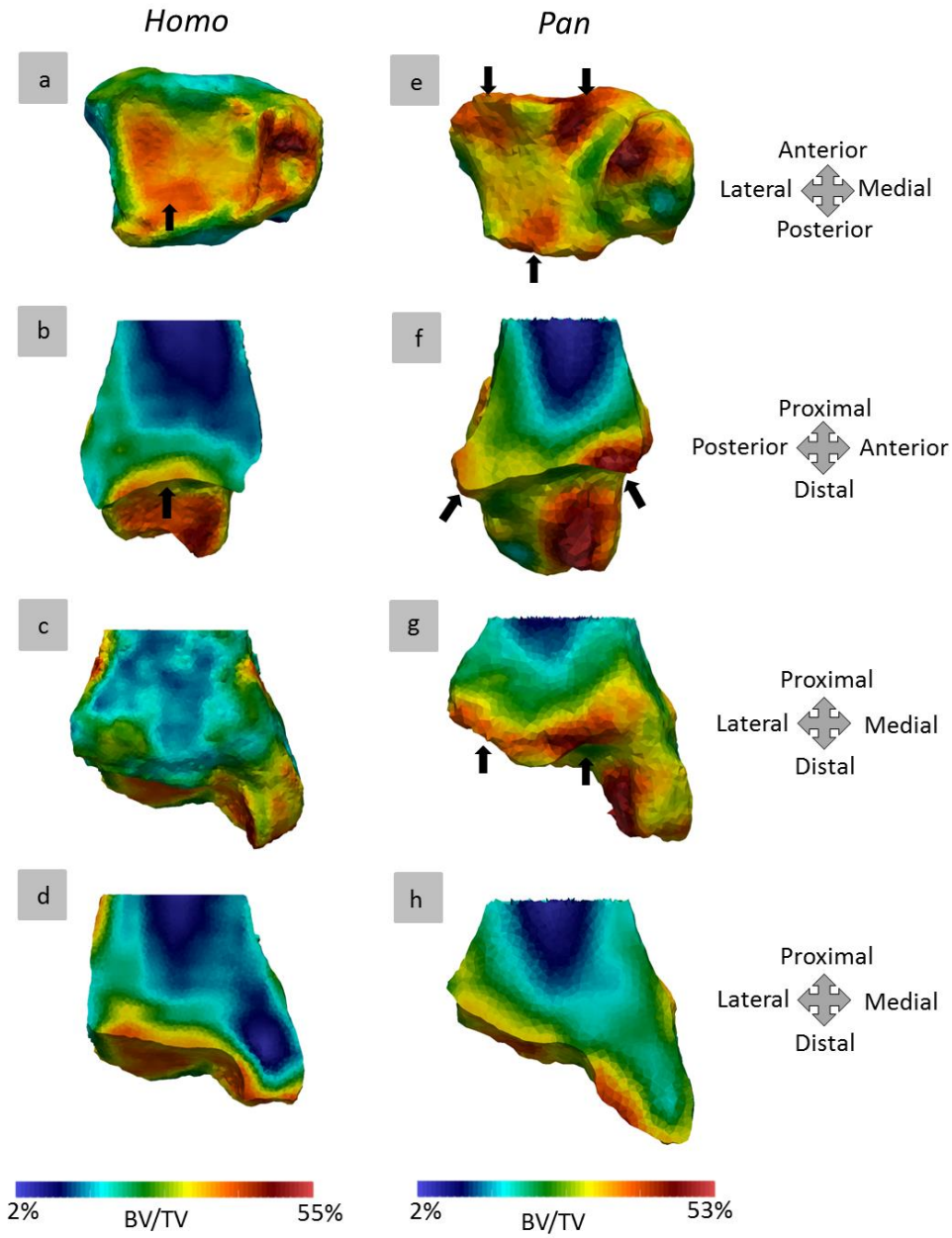

Fig 9. Morphometric maps of mean relative cortical thickness on the canonical talus in *Homo* (a) and *Pan* (b) in (from left to right) anterior, dorsal and plantar views. Red indicates thick regions and blue indicates thin regions. (c) Differences between the species are shown as the difference in *Pan* compared to *Homo* with positive values (red) indicating thicker bone and negative values (blue) indicating thinner bone. (d) Regions of significant differences between the species at vertices and clusters (red-yellow) and at clusters (blue) of the surface mesh.

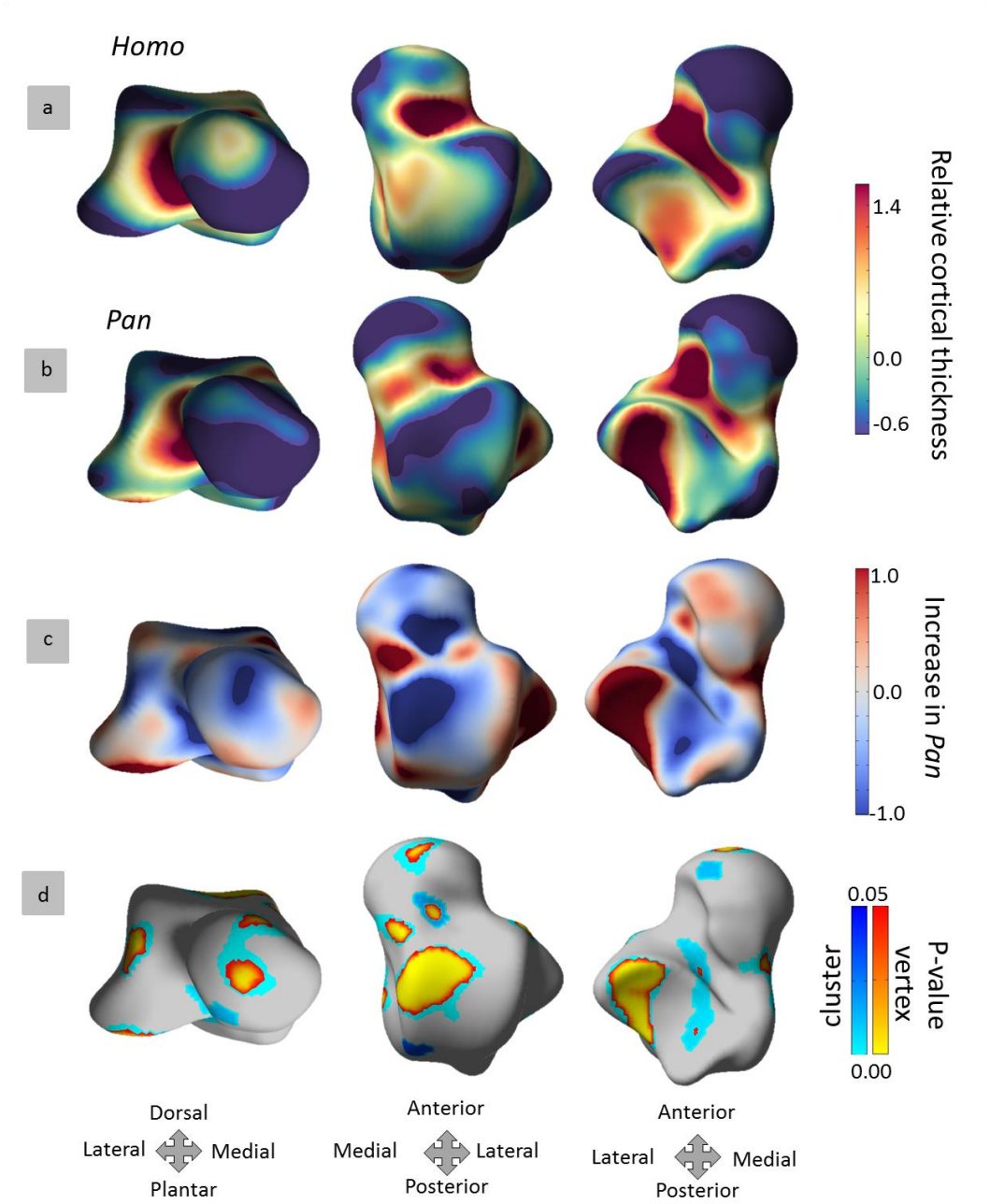

Fig 10. Morphometric maps of mean relative cortical thickness on the canonical tibia in (a) *Homo* and (b) *Pan* in (from left to right) lateral, distal and anterior views. Red indicates thick regions and blue indicates thin regions. (c) Differences between the species are shown as the difference in *Pan* compared to *Homo* with positive values (red) indicating thicker bone and negative values (blue) indicating thinner bone. (d) Regions of significant differences between the species at vertices and clusters (red-yellow) and at clusters (blue) of the surface mesh.